Coupled numerical and theoretical study of the flow transition between a rotating and stationary disk

Eric Serre, Ewa Tuliszka-Sznitko, Patrick Bontoux

Coupled numerical and theoretical study of the flow transition between a rotating and a stationary disk

Eric Serre[a)]
LMSNM CNRS-FRE 2405, IMT Château-Gombert, La Jetée, Université de la Méditerranée, 38 rue F. Joliot-Curie, 13451 Marseille Cedex 20, France

Ewa Tuliszka-Sznitko
Institute of Thermal Engineering, Technical University of Poznan, 60-965 Poznan, Poland

Patrick Bontoux
LMSNM CNRS-FRE 2405, IMT Château-Gombert, La Jetée, Université de la Méditerranée, 38 rue F. Joliot-Curie, 13451 Marseille Cedex 20, France

(Received 6 March 2003; accepted 20 November 2003; published online 4 February 2004)

Both direct numerical simulation and theoretical stability analysis are performed together in order to study the transition process to turbulence in a flow between a rotating and a stationary disk. This linear stability analysis considers the complete rotor-stator flow and then extends the results of Lingwood [J. Fluid Mech. **299**, 17 (1995); **314**, 373 (1996)] obtained in a single disk case. The present linear analysis also extends the former two-disk computations of Itoh [ASME FED **114**, 83 (1991)], only limited to a hydrodynamic spatial instability analysis. Moreover, in the present work, this approach is completed by discussing the effects of buoyancy-driven convection on the flow stability and by absolute/convective analysis of the flow. Coupled with accurate numerical computations based on an efficient pseudo-spectral Chebyshev–Fourier method, this study brings new insight on the spatio-temporal characteristics of this flow during the first stages of transition. For instance, an exchange of stability from a steady to a periodic flow with spiral structures is observed for the first time numerically in such cavity of large aspect ratio. The nature of the first bifurcation is discussed as well as the influence on it of disturbances coming from the end-wall boundary layer. Annular and spiral patterns are observed in the unstable stationary disk layer with characteristic parameters agreeing very well with the present theoretical results. Then, these structures are interpreted in terms of type I and type II generic instabilities. Moreover, the absolute instability regions which are supposed to be strongly connected with the turbulent breakdown process are also identified and the critical Reynolds numbers of the convective/absolute transition in both Ekman and Bödewadt layers are given.
[DOI: 10.1063/1.1644144]

I. INTRODUCTION

Flows in rotating disks system are not only a subject of fundamental interest as prototype flows with three-dimensional boundary layers but are also a topic of practical importance in the performances improvement of many industrial devices. Typical configurations are cavities between rotating compressors and turbines disks.[1] Numerous works have been recently devoted to the investigation of the instabilities associated to a single disk flow[2–5] and to a differentially rotating disks flow.[6–10] Identification and characterization of mechanisms related to this process should improve the prediction methods and lead to new, more efficient control strategies, of considerable importance in practical flows. Despite intensive work and recent advances, no full understanding of the transition and the turbulent breakdown process has yet been achieved in these flows.

In the limit of high rotation rate, the flow between a rotating and a stationary infinite disk is of Batchelor type and presents two separated layers by an inviscid rotating core: of Ekman type on the rotating disk and of Bödewadt type on the stationary disk. The transition process in both these layers is related to type I and type II generic linear instabilities which have been extensively experimentally and theoretically documented (see a review in Ref. 11). The type I instability, also referred as ''cross-flow'' instability, is due to the presence of an unstable inflection point in the boundary layer velocity profile. The mechanism for type II instability is related to the combined effects of Coriolis and viscous forces (see details in Ref. 12). The spatial structure of both instabilities consists of traveling vortices in the boundary layers expanding in rings or spirals in the azimuthal direction. Faller[13] and Caldwell and Van Atta[14] have investigated experimentally the type I and type II instabilities in the Ekman flow and found reasonably good agreement with linear stability theory. Savas[15] studied experimentally unsteady uniformly rotating flow over a stationary disk and found both rings and spiral structures recognized as the type II and type I instability, respectively. In both rotor/stator cavity flow and Ekman and

a)Electronic mail: serre1@l3m.univ-mrs.fr

Bödewadt flows around a single disk, the experimental results exhibit the similar instability structure; however, the confinement of the geometry (rotor/stator geometry) has effect on the critical Reynolds number.[9]

A more recent insight on the transition process in these boundary layers has been carried out by considering the response to a brief and localized perturbation introduced into the unstable boundary layer region. When an impulse response grows with time at every location in space, the flow is defined as absolutely unstable.[16,17] By contrast, when the response decays at every location in a sufficiently long time, the flow is defined as convectively unstable. The convective/absolute nature of the transition in the Ekman family flows on the single rotating disk has been evidenced in both theoretical and experimental studies.[3,4,18] In a very recent work, Pier[5] has carried out a secondary stability analysis of a single rotating disk boundary layer which has revealed that as soon as the primary nonlinear waves come into existence they are already absolutely unstable with respect to secondary perturbations. This theoretical result shows that the secondary disturbances continuously perturb the primary vortices, thus involving the direct route to turbulence. A convective/absolute transition has been also experimentally revealed by Gauthier *et al.*[6] in a flow between a stationary and a rotating disk in a rotor/stator cavity.

The flow between two disks rotating in the rotor/stator configuration has been analyzed with the assumption that the radius of the disks is either infinite[7,19] or finite.[9,10] In the case of the finite radius of the disks, additional parameters are needed to describe the geometrical configuration, namely, the ratio of the radial extension to the distance between the disks and also to described imposed boundary conditions. The modification brought by the presence of an external shroud, the influence of the attachment of the shroud to the rotor or to the stator, and the influence of the approximation of the azimuthal outer radius velocity profile have been discussed in different papers.[20–23] Great influence of the end-wall boundary layer on the flow structure has been reported.

In our former studies, rotor-stator flows were investigated in time-dependent regimes above the threshold[9] or even in transitional turbulent regimes.[24] In the present paper, the first stages of the transition process have been more accurately investigated, using coupled theoretical and numerical investigations. In cylindrical cavities of small aspect ratio[9,22] ($L=2$) or in a tank with a rotating lid,[25] the transition process to unsteadiness is clear. Increasing rotation step by step, a critical Reynolds number is found beyond which the flow becomes nicely periodic and then successive bifurcations ultimately lead to chaos. Surprisingly, in cylindrical cavities of larger aspect ratio ($5 \leqslant L \leqslant 10$) such bifurcations scenario has never been reported numerically until now, excepted in 2D calculations by Hadid,[26] and the transition to unsteadiness was only obtained as a direct transition from a steady to a chaotic state.

The three-dimensional direct numerical calculations (DNS), based on high-order spectral methods, are carried out in a cylindrical rotor-stator cavity of aspect ratio $L(R_1/2h) = 5$. The high accuracy of the numerical method, involving a full control of the flow in this simple geometry, allows an accurate description and characterization of the different flow structures related to boundary layer instabilities. In contrast to former studies quoted above, the slow increase of the rotating disk velocity and a careful analysis of the results has allowed us to emphasize a nice supercritical Hopf bifurcation associated with the occurrence of vortices in the stationary disk layer (Bödewadt type).

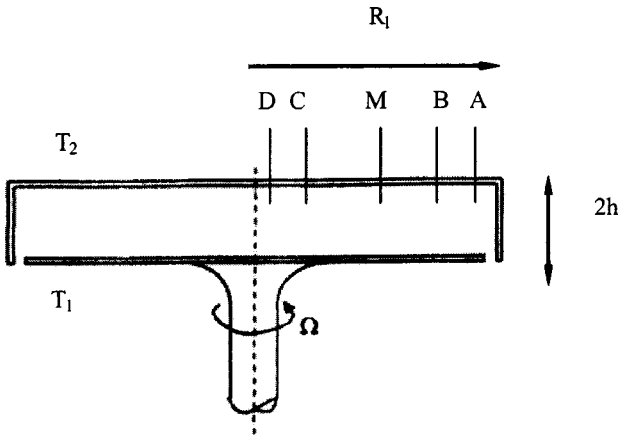

FIG. 1. Schematic picture of the rotating cavity of radius R_1 and height $2h$ with marked monitoring points in radial direction. In the non-isothermal configurations, T_1 and T_2 are the temperatures of the rotating and of the stationary disk, respectively.

A linear local stability analysis (LSA) is also performed in order to enlighten the DNS results with respect to type I and type II instability. The characteristic parameters of the vortex structures obtained by the DNS method compare favorably with LSA results. Moreover, the absolute instability regions are theoretically identified, extending the approach of Lingwood[3,4] for a single disk to the two disks rotor/stator flow. The absolute/convective character of the flow is also discussed in the light of our DNS calculations. Then, buoyancy-driven convection effects on the flow stability are analyzed by extending LSA calculations to the case of non-isothermal flows.

This article is organized as follows. In Sec. II, the geometrical configuration considered in DNS and the governing parameters are described. Then, in two next sections the governing equations with the boundary conditions are given and the main features of the LSA and DNS methods are outlined. In Sec. V, isothermal LSA results are presented together with non-isothermal LSA results where the buoyancy-driven convection is enhanced by the density variation via a Boussinesq approximation in the centrifugal acceleration field. Moreover, the absolute/convective character of the flow is discussed in both isothermal and non-isothermal cases. In Sec. VI, the DNS results are analyzed in the case of rotation-driven isothermal flows. Finally, discussion and concluding remarks are made in Sec. VII.

II. GEOMETRICAL MODEL AND PHYSICAL PARAMETERS

The geometrical model is a rotor-stator cylinder of radius R_1, bounded by a stationary cylinder of height $2h$ (Fig. 1). In this study, the aspect ratio of the cavity $L=(R_1/2h)$

$=5$ is a compromise between actual rotor/stator devices and computational cost required by time-dependent three-dimensional calculations. The rotor rotates at uniform angular velocity $\Omega=\Omega e_z$, e_z being the unit vector. The origin of the z-axis is located at the mid-height between the disks.

The flow is controlled by two physical parameters which are the Reynolds number, Re, and the aspect ratio, L. The closed geometry is characterized by two independent length scales, R_1 and h, each of which is used in the literature in the definition of Re. In this article, the Reynolds number based on the external radius of the disks, $\mathrm{Re}_R=R_1^2\Omega/\nu$, has been chosen (used among others by Owen and Rogers[1] and Lopez and Weidman).[23] For sufficiently large rotation rate, both layers can be studied independently as a first approach as the flow over a single disk. In the rest of the article, both layers will be referred to as stationary disk and rotating disk layer in the two disks configuration, in contrast to Bödewadt and Ekman layer, respectively, in a single disk flow case. In this case, the relevant parameter is the local Reynolds number, $\mathrm{Re}_\delta=r^*/\delta=(r^{*2}\Omega/\nu)^{1/2}$, based on the local distance to the axis and the viscous scale $\delta=(\nu/\Omega)^{1/2}$. We notice that Re_R is an upper bound to the square of Re_δ. This local Reynolds number is relevant to discuss the instability thresholds and characteristic parameter of the instability waves.

For non-isothermal flows, considered in LSA, we have additional governing parameters, i.e., the thermal Rossby number $B=\bar{\beta}(T_2-T_1)$, where $\bar{\beta}=-1/\rho_r(\partial\rho/\partial T)_P$ is the thermal-expansion coefficient and T_1, T_2 are the temperatures of the rotating and stationary disks, respectively.

III. MATHEMATICAL MODEL AND NUMERICAL METHOD (DNS)

The governing equations are the 3D Navier–Stokes equations, written in velocity-pressure formulation together with the continuity equation. The equations are written below in a cylindrical polar coordinate system (r,z,φ), with respect to a stationary frame of reference:

$$\frac{\partial V}{\partial t}=\frac{1}{\mathrm{Re}}\Delta V-(V\cdot\nabla)V-\nabla p,$$

$$\nabla\cdot V=0,$$

where t is the time, V is the velocity vector, (u,w,v) are the velocity components in r, z, and φ directions, respectively, and p is pressure.

The scales for the dimensionless variables of time, space, and velocity are Ω^{-1}, h and ΩR_1, respectively. The dimensionless axial coordinates are $z=z^*/h$; $z\in[-1,1]$ (asterisks denote the dimensional values). The radius coordinate is normalized to obtain the domain $[-1, 1]$ requested by the spectral method, based on the Chebyshev polynomials: $r=(2r^*-R_1)/R_1$. No slip boundary conditions apply at all rigid walls; then $u=w=0$. For the azimuthal velocity component, the boundary conditions are $v=0$ on the stator and $v=(1+r)/2$ on the top rotating disk. The end-wall cylinder is also supposed at rest, then $v=0$. However, in order to eliminate the singularity of the azimuthal velocity at the junction between the stationary end-wall and the rotating disk, this boundary condition is smoothed using an exponential azimuthal velocity profile $v=\exp((z-1)/0.006)$ which approximates well the thin gap between the edge of the rotating disk and the stationary end-wall. The initial condition is as follows: $u=0$, $v=(1+r)(z+1)/4$, $w=0$.

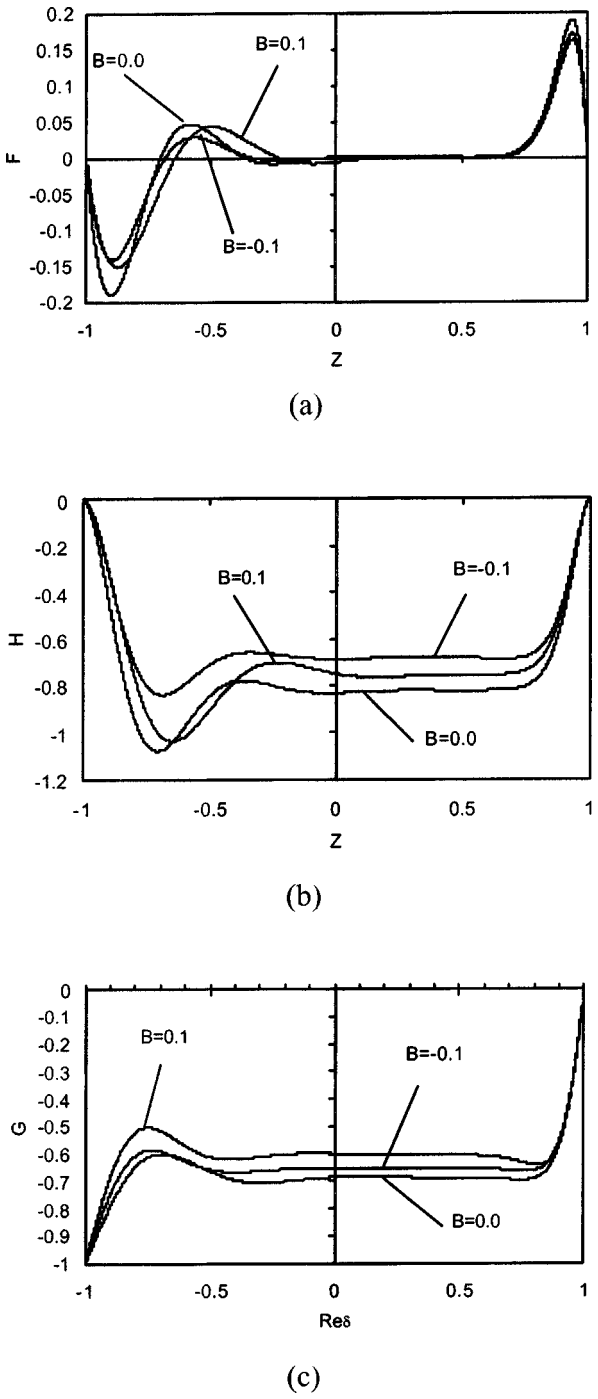

FIG. 2. Similarity solutions of Batchelor type at $\mathrm{Re}=1000$ ($\mathrm{Re}=\Omega(2h)^2/\nu$) and for three different Rossby numbers: $B=0.1$ (cooling of the rotating disk), 0 (isothermal) and -0.1 (cooling of the stationary disk). Profiles of the radial ($F=u^*/\Omega r^*$) (a), axial $H=w^*/\sqrt{\nu\Omega}$ (b), and azimuthal ($G=v^*/\Omega r^*$) (c) velocity components.

The numerical solution is based on a pseudospectral collocation Chebyshev–Fourier Galerkin approximation.[27] The use of the Gauss–Lobatto collocation points, corresponding

TABLE I. Characteristic parameters of the type II instability of the Bödewadt flow and of the stationary disk boundary layer. Present DNS and LSA results and literature results.

Authors	Re_δ	ε	λ_r	$V_\phi^*/\Omega r^*$	$\mathrm{Re}_{\delta\mathrm{II}}$	σ
Feria (Ref. 33), PST	19.8[a]	0.0°	12.3	−0.22	19.8	2.1
Itoh (Ref. 7), LSA	[38.6; 55]	[−29.8°; −25.6°]	[34; 34.8]	[−0.23; −0.21]	38.6	[1.9; 2.3]
Savas (Ref. 15), Exp.	35	0.0°	19	−0.1	35	1.15
Serre (Ref. 9) DNS, $L=2$	[21; 126.5]	0.0°	[10; 21]	[−0.08; −0.02]	21	0.9
Serre (Ref. 9) DNS, $L=5$	[27; 173]	0.0°	[8; 17]	[−0.13, −0.21]	27	4
			Present results			
LSA stationary disk layer	[34.7; 62]	[−34.6°, −31.3°]	[35.1; 35.7]	[−0.25, −0.23]	34.7	[1.9; 2.8]
LSA Bödewadt	18.9[a]	−27.38	16.11	−0.67	18.9	5.59
DNS, $L=5$, $\eta=0.0$	[25.8; 62]	0.0°	[7.3; 16.2]	[−0.01; 0.022][b]	25.8	1.1
DNS, $L=5$, $\eta=3.5$	[23.4−74.6]	−15.0°	[9.3; 14.25]	[−0.0032; −0.002][b]	23.4	1.55

[a]In these cases the local Reynolds number is based on the viscous length calculated with the velocity of the fluid at infinity and not with the disk velocity.
[b]These values correspond to the radial phase speed.

to the extrema of the Chebyshev polynomials Tn and Tm of high degree, N and M in the radial and axial directions, respectively, directly ensures high accuracy of the solution inside the very narrow wall layers. The differential equations are exactly satisfied at the Gauss–Lobatto collocation points $(r_i, z_j) \in [-1,1]\times[-1,1]$, with $r_i = \cos(i\pi/N)$ and $z_j = \cos(j\pi/M)$ for $i=0,...,N$ and $j=0,...,M$.

The approximation of the flow variables $\psi=(u,w,v,p)$ is given by a development in truncated series:

$$\Psi_{\mathrm{NMK}}(r,z,\varphi,t) = \sum_{p=-K/2}^{K/2-1} \sum_{n=0}^{N} \sum_{m=0}^{M} \Psi_{\mathrm{nmp}}(t) T_n(r) T_m(z) e^{ip\varphi}$$

$$\text{for} \quad \begin{matrix} -1 \leqslant r,z \leqslant 1, \\ 0 \leqslant \varphi \leqslant 2\pi. \end{matrix}$$

The derivatives are obtained from

$$\frac{\partial^q \Psi_{\mathrm{NMK}}}{\partial r^q}(r_i,z_j,\varphi_k,t) = \sum_{\eta}^{N} dr_{i\eta}^{(q)} \Psi_{\mathrm{NMK}}(r_\eta,z_j,\varphi_k,t),$$

$$\frac{\partial^q \Psi_{\mathrm{NMK}}}{\partial z^q}(r_i,z_j,\varphi_k,t) = \sum_{\xi}^{M} dz_{j\xi}^{(q)} \Psi_{\mathrm{NMK}}(r_i,z_\xi,\varphi_k,t),$$

where $dr_{ij}^{(q)}$, $dz_{ij}^{(q)}$ correspond to the coefficients of the matrix of the first and second derivatives $(q=1,2)$ and where $\varphi_k = 2\pi/K$, $k=0,...,K-1$ are points in azimuthal direction.

The singularity introduced by the axis at $r=0$ has required a dependent variable transformation $\tilde{V}=rV$, $\tilde{p}=rp$ as proposed by Serre and Pulicani.[28]

The time scheme is semi-implicit and second-order accurate. It corresponds to a combination of the second-order backward differentiation formula for the viscous diffusion term and the Adams–Bashforth scheme for the nonlinear terms. The method uses a projection scheme to maintain the incompressibility constraint.[27–29]

IV. LINEAR STABILITY ANALYSIS (LSA)

The disturbance equations are obtained by expressing the velocity, temperature, and pressure fields as the superposition of the basic state and of a perturbation field. Once the non-isothermal flow condition is considered, the thermal effects and the rotational-induced buoyancy become important and influential in stability characteristics and the critical conditions. In order to take into account the buoyancy effects the Boussinesq approximation is invoked, i.e., the density asso-

TABLE II. Characteristic parameters of the type I instability of the Bödewadt flow and of the stationary disk boundary layer. Present DNS and LSA results and literature results.

Authors	Re_δ	ε	λ_r	$V_\phi^*/\Omega r^*$	$\mathrm{Re}_{\delta\mathrm{I}}$	σ
Itoh (Ref. 7), LSA	[48.1; 200]	[−1.6°; 14°]	[23.7; 24.16]	[−0.077; −0.02]	48.1	0.98
Lingwood (Ref. 4)	27.4[a]	13.3°	13	0	27.4	0.0
Serre (Ref. 9) DNS, $L=2$	[63.2; 126.5]	[7°; 25.7°]	[28.5; 16.1]	[−0.062; −0.68]	63.5	[0.9; 2.8]
Serre (Ref. 9) DNS, $L=5$	[86.5; 173]	[7°; 28°]	[8.8; 17]	[−0.02; −0.27]	86.5	1
			Present results			
LSA stationary disk layer	[47.5; 200]	[0.8°, 10°]	[21.2; 24.35]	[−0.062, −0.018]	47.5	0.9
DNS, $L=5$	52.5	12.1°	[4.4; 14.7]	[−0.020; −0.006][b]	52.5	1

[a]In these cases the local Reynolds number is based on the viscous length calculated with the velocity of the fluid at the infinity and not with the disk velocity.
[b]These values correspond to the radial phase speed.

TABLE III. Characteristic parameters of the type II instability of the Ekman flow and of the rotating disk boundary layer. Present LSA results and literature results.

Authors	Re_δ	ε	λ_r	$V_\phi^*/\Omega r^*$	$\mathrm{Re}_{\delta\&\mathrm{II}}$	σ
Melander (Ref. 38), Ekman LSA	54.15	−23.3°	21.64	0.616	54.15	10.54
Itoh (Ref. 7), Ekman LSA	54.2	−23.3°	21.65	0.616	54.2	10.55
Itoh (Ref. 7), LSA rotating disk layer	85.3	−24.7°	26.91	0.373	85.3	8.17
Present results						
LSA rotating disk layer	90.23	−26.3°	28.56	0.39	90.23	8.73
LSA Ekman flow	54.18	−23.4°	21.66	0.617	54.18	10.56

ciated with the gravity terms, the centrifugal and the Coriolis forces due to the disk rotation, and the curvilinear motion of the fluids are all considered as variable.

A similarity model of the thermal flow is used for generating axially symmetric solutions of the basic state.[30] Dimensionless radial profiles ($F=u^*/\Omega r^*$), axial ($H=w^*/\sqrt{\nu\Omega}$) and azimuthal ($G=v^*/\Omega r^*$), are presented in Fig. 2 ($\mathrm{Re}=\Omega(2h)^2/\nu=1000$) for three different thermal Rossby numbers. Thermal effects on this base flow will be discussed in Sec. V. As in Ref. 7, the flow is of Batchelor type and the solid-body angular velocity is constant and equal to $v^*/\Omega r^*=-0.687$ [Fig. 2(c)] in the rotating frame of reference. This speed ratio can define a Rossby number, Ro, between convective and Coriolis effects.

We assume that the perturbation quantities have the following normal-mode form:

$$[u',v',w',p',\tau']^T=[\hat{u},\hat{v},\hat{w},\hat{p},\hat{\tau}]^T\exp(\alpha^* r^*+m\varphi-\omega^* t^*)+\mathrm{cc},$$

where $\hat{u}$, $\hat{w}$, $\hat{v}$, $\hat{p}$, $\hat{\tau}$ are the dimensional amplitudes of the three components of velocity (in r^*, z^*, φ directions), pressure, and temperature, respectively, α^* and $\beta^*=m/r^*$ are the components of wave number k^* in the radial and azimuthal directions, respectively, ω^* is the frequency, and t^* is time. The coordinate system is located on the disk under consideration. The linear local stability analysis equations plus the homogeneous boundary conditions $\hat{u}(z^*)=\hat{v}(z^*)=\hat{w}(z^*)=\hat{\tau}(z^*)=0$ at $z^*=-h$ and $z^*=h$ constitute an eigenvalue problem which is solved in a global manner.[30] As in the DNS computations, a spectral collocation method based on Chebyshev polynomials is used for discretization of the LSA equations.

LSA is also used to determine the absolute/convective character of the boundary layers using the Briggs[16] criterion. Following the review paper of Huerre,[17] the flow is defined as absolutely unstable if its impulse response grows with time at every location in space. The response of a linear system to the forcing input can be determined by the Green function $G(x,t)$:

$$G(x,t)=\frac{1}{(2\pi)^2}\int_F\int_L\frac{e^{i(kx-\omega t)}}{D(k,\omega;\mathrm{Re}_\delta)}d\omega\,dk.$$

Path F in the complex plane of wave number k is initially taken to be the real axis. The contour L in the complex frequency plane ω is chosen so that the causality is satisfied: $G(x,t)=0$ everywhere when $t<0$. From the asymptotic solution of the Fourier–Laplace integral, a general mathematical criterion has been derived to determine the nature of instability.[16,17,31,32] According to this criterion, the absolute instability can be identified by singularities in the dispersion relation, called pinch-points. The pinch-points are found in a process of consecutive contour deformations in which L is deformed toward the lower half of the ω plane.[32] We have the following criteria for absolute instability: the flow is absolutely unstable if the so-called absolute amplification rate ω_{oi} is positive ($\omega_{oi}>0$). Additionally, for L contour located high enough in the ω-plane the spatial branches $k^+(\omega)$ and $k^-(\omega)$ must lie in different halves of the k-plane.

For all flows, except the Ekman single disk boundary layer which is parallel in the strict sense, the parallel flow assumption is used in the LSA. It is expected that the parallel flow assumption have no large influence on numerical results and that general instability characteristics reveal the general features of the flow. For example, in the Karman flow,

TABLE IV. Characteristic parameters of the type I instability of the Ekman flow and of the rotating disk boundary layer. Present LSA results and literature results.

Authors	Re_δ	ε	λ_r	$V_\phi^*/\Omega r^*$	$\mathrm{Re}_{\delta\&\mathrm{I}}$	σ
Melander (Ref. 38)	112.76	7.2°	11.49	0.094	112.76	5.84
Lingwood (Ref. 4), Ekman	116	14.5°	11.89	0.0	116	0.0
Itoh (Ref. 7), LSA Ekman	113	7.2°	11.49	0.094	113	5.85
Itoh (Ref. 7), LSA rotating disk layer	281	10.9°	15.307	0.0185	281	2.17
Present results						
LSA rotating disk boundary layer	278.6	10.9°	15.056	0.0185	278.6	2.19
LSA Ekman flow	112.78	7.2°	11.49	0.094	112.78	5.84

TABLE V. Characteristic parameters of type I and type II instabilities of the rotating disk layer in non-isothermal flow.

		Present results		
B	λ_r	ε	$V_\phi^*/\Omega r^*$	$\mathrm{Re}_{\delta c}$
Type II				
−0.1	26.69	−24.895	0.36	94.8
−0.06	27.14	−25.26	0.370	93.42
−0.02	27.8	−26.048	0.382	91.46
0	28.26	−26.3	0.39	90.23
0.02	28.95	−25.95	0.385	67.2
0.06	30.77	−25.873	0.3826	110.19
0.1	32.73	−26.1	0.3846	121.9
Type I				
−0.1	14.58	10.5	0.022	281.3
−0.06	14.73	10.65	0.0189	280
−0.02	14.98	10.8	0.0188	279.15
0	15.055	10.9	0.0184	278.6
0.02	14.937	10.5	0.0247	271.655
0.06	14.544	9.5	0.0382	257.02
0.1	14.41	8.1	0.05395	243.04

TABLE VI. Characteristic parameters of type I and type II instabilities of the stationary disk layer in non-isothermal flow.

		Present results		
B	λ_r	ε	$V_\phi^*/\Omega r^*$	$\mathrm{Re}_{\delta c}$
Type II				
−0.1	30.22	−23.68	−0.2226	46.46
−0.06	31.84	−26.77	−0.2302	42.84
−0.02	34.14	−32.00	−0.2460	38.15
0	35.32	−35.32	−0.2526	34.69
0.02	36.01	−37.02	−0.2705	35.41
0.06	37.20	−39.88	−0.2972	35.64
0.1	37.52	−41.91	−0.3216	35.93
Type I				
−0.1	20.68	2.3	−0.0560	61.0
−0.06	20.46	0.2	−0.0646	55.95
−0.02	20.88	−1.2	−0.0767	50.38
0	21.20	−0.8	−0.0787	47.5
0.02	20.20	0.85	−0.0849	46.80
0.06	18.99	4.77	−0.0975	45.79
0.1	18.32	7.73	−0.1200	45.27

Lingwood[3,4] demonstrated that both theoretical and experimental critical Reynolds numbers of absolutely unstable flow coincide. Moreover, using linear parabolized stability theory including nonparallel effects, Feria[33] obtained a critical Reynolds number of the Bödewadt layer type II instability (single disk), $\mathrm{Re}_\delta = 19.8$, very close to the one obtained in the present study, $\mathrm{Re}_\delta = 18.9$ (see Table I). We can also expect that for two-disk model the error caused by nonparallel effects is not significant. Even if nonparallel effects due to radial confinement could explain the slight disagreements observed with our DNS results, the parallel flow studies provide qualitatively correct descriptions of the investigated class of flows and are very helpful in interpretation of DNS results in terms of type I and type II instability and in determining the absolute/convective character of the boundary layer flow.

V. LINEAR STABILITY ANALYSIS RESULTS

Our linear stability analysis considers the complete rotor-stator flow (disks of infinite radius) for both isothermal and non-isothermal configurations. We focus here on the characteristics of the instabilities which were shown to be the most unstable. All these LSA results are summarized in Tables I–VIII together with present DNS and available literature results.

A. Type I and type II boundary layer instabilities

Characteristic parameters of the type I and type II instability are given for isothermal flows in Tables I–IV, for the both stationary (I, II) and rotating boundary layer flows (III, IV). The thermal effects on the instabilities characteristics are summarized in Tables V and VI. The main spectral parameters are normalized as follow: the wave-number k's components in radial and azimuthal directions are $\alpha = \alpha^* \delta$, $\beta = \beta^* \delta$, the phase speed $V_\phi = V_\phi^*/\Omega r^* (= \omega_r / k)$ and the frequency $\sigma = \omega\, \mathrm{Re}$.

1. Isothermal flow

a. Stationary disk boundary layer. In the stationary disk layer, the onset of the type II instability has been found at $\mathrm{Re}_{\delta \mathrm{II}} = 34.7$ and with a negative phase speed $V_\phi = -0.2526$ showing that the disturbances propagate in the stationary disk flow direction. The present research shows that type II instability only exists in a narrow range of Re_δ, disappearing at $\mathrm{Re}_\delta = 62$. Type I instability occurs at a slightly larger Reynolds number, $\mathrm{Re}_{\delta \mathrm{I}} = 47.5$. The exemplary iso-lines of the temporal amplification rate obtained at different $\mathrm{Re}_\delta = 65$, 80, and 130 are shown in the plane of the wave-angle and wave-number in Figs. 3(a)–3(c) in order to show the area of dominant type I and type II instability with respect to the Re_δ. On the stationary disk at $\mathrm{Re}_\delta = 65$, two separate regions of instability exist [Fig. 3(a)]. The first peak obtained for higher wave-number with the maximum at $k \sim 0.28$ and $\varepsilon \sim 5°$ is identified as the type I instability. The second peak with the maximum at $k \sim 0.2$ and $\varepsilon \sim -30°$ corresponds to the type II instability. As expected only the type I instability exists at $\mathrm{Re}_\delta = 80$ and 130 [Figs. 3(b) and 3(c)].

Our type I and type II isothermal linear stability results of the stationary disk boundary layer are in very good accordance with the experimental results of Savas,[15] who obtained $\mathrm{Re}_{\delta \mathrm{II}} = 35.0$ and with the theoretical results of Itoh[7] (Tables I and II). The small deviation from Itoh's results, in the critical Reynolds numbers, can be attributed to the use of two different numerical procedures and computational facilities.

b. Rotating disk boundary layer. Our results show that the rotating disk layer is much more stable than the stationary disk boundary layer discussed above. Indeed, the onset of type II instability has been found at $\mathrm{Re}_{\delta \mathrm{II}} = 90.23$ and of type I at $\mathrm{Re}_{\delta \mathrm{I}} = 278.6$.

Our critical parameters are in very good agreement with Itoh's[7] results (see Tables III and IV). The critical parameters of the type I instability are also in good agreement with the critical parameters obtained by Lingwood[18] for the Ekman layer (stationary waves, $V_\phi = 0.0$) on a single disk. However,

TABLE VII. Critical parameters of the absolutely unstable area in the Bödewadt flow and in the stationary disk boundary layer.

Authors	$\mathrm{Re}_{\delta\&a}$	α_r	α_i	β	ω_r
Lingwood (Ref. 4), LSA Bödewadt	21.6[a]	0.34	0.0776	−0.1174	−0.218
	Present results				
LSA Bödewadt	21.7[a]	0.34	0.0806	−0.1124	−0.2132
LSA stationary disk layer	48.5	0.19	0.0569	−0.0316	−0.0277

[a]In these cases the local Reynolds number is based on the viscous length calculated with the velocity of the fluid at the infinity and not with the disk velocity.

there is a large difference between our critical Reynolds number of the type I instability, $\mathrm{Re}_{\delta\mathrm{I}}=278.6$ (also Itoh's result,[7] $\mathrm{Re}_{\delta\mathrm{I}}=281$) and that obtained by Lingwood,[18] $\mathrm{Re}_{\delta\mathrm{I}}=116.3$, for the Ekman boundary layer on a single disk. This discrepancy is attributed to the influence of the stationary disk in the two-disk configuration as opposed to the open domain in Lingwood's Ekman flow. Indeed, as underlined in Sec. IV of the present work the Rossby number Ro is not equal to zero as in the Ekman layer studied by Lingwood.[18] Then, a more relevant comparison would be certainly given by interpolating the Lingwood result for Rossby equal to -0.751 which is closer to $\mathrm{Ro}=-1$ (Karman layer) than $\mathrm{Ro}=0$ (Ekman layer). Unfortunately, data required for precise interpolation are missing in Lingwood's work.

2. Non-isothermal flow

In order to analyze the effect of thermal conditions on the instability characteristics, we have extended our investigations to the non-isothermal class of flow. Calculations have been performed for different thermal Rossby numbers $B=\tilde{\beta}(T_2-T_1)$; however, for validity of the Boussinesq approximation, the values of B have been limited in this study to a small range, e.g., $-0.1\leqslant B\leqslant 0.1$. From the definition of the thermal Rossby number, the positive and negative values of B stand for $T_2>T_1$ (cooling of the rotor wall) and $T_2<T_1$ (cooling of the stator wall), respectively. When the stator is cooled ($B<0$), buoyancy enhances in the rotor-stator cavity, a secondary flow which develops in opposite direction to the basic recirculation. In contrast, when the rotor wall is cooled ($B>0$), the buoyancy driven secondary flow enforces the basic rotation driven flow.

Tables V and VI give the instability characteristic parameters of the rotating and stationary disk boundary layer, respectively, for the varying thermal Rossby number. In the frame of the variations of B within the $\pm 10\%$ range of empirical validity of the Boussinesq approximation, interesting details on the unstable flow are presented. For both type I and type II instabilities, the changes in the characteristics parameters are larger in the stationary than in rotating boundary layer for B varying from -0.1 to 0.1, showing that thermal buoyancy effects are stronger in the stator boundary layer. This behavior is certainly related to the relative influence of the thermal buoyancy with respect to the rotation buoyancy driven which is larger in the stationary disk layer than in the rotating disk layer.

a. Stationary disk boundary layer. The type I and II critical Reynolds numbers are shown in Fig. 4(a) versus B for the stationary disk boundary layer. As we can see from Fig. 2, the influence of the thermal Rossby number on the radial velocity profiles in the stationary disk boundary layer is stronger than on the rotating disk boundary layer.

The influence of heating ($B>0$) is small. The boundary layer of the stationary disk turned out to be more unstable than that of the rotating disk for all considered values of B. All the type II characteristic parameters ($\lambda_r,\varepsilon,V_\phi$) increase comparatively to the isothermal case while for the type I, the wavelength slightly decreases, and the inclination and the phase velocity strongly increases. An important feature is the change in the spiral inclination from a negative angle in the isothermal case ($-0.8°$) to a positive one as soon the rotor starts to be cooled ($\varepsilon=0.85, B=0.02$).

The cooling of the stationary disk ($B<0$) stabilizes the flow with respect to both type I and type II instabilities [Fig. 4(a)] by increasing the critical Reynolds numbers when B is

TABLE VIII. Critical parameters of the absolutely unstable area in the Ekman, von Karman, rotating disk layer flows and in flows for two Rossby numbers $=-0.8$ and -0.6.

Authors	$\mathrm{Re}_{\delta\&a}$	α_r	α_i	β	ω_r
Lingwood (Ref. 4) LSA, Ekman	198	0.379	±0.195	0.184	±0.0397
Lingwood (Ref. 4) LSA, von Karman	507.3	0.217	−0.122	0.135	−0.0349
Lingwood (Ref. 4) LSA, Ro=−0.8	434.8	−0.252	−0.142	0.155	0.0393
Lingwood (Ref. 4) LSA, Ro=−0.6	345.4	−0.294	−0.164	0.169	0.0418
	Present results				
LSA Ekman flow	198	0.379	±0.195	0.184	±0.0397
LSA rotating disk layer. Ro=−0.687	562	0.26	−0.1429	0.152	−0.0258

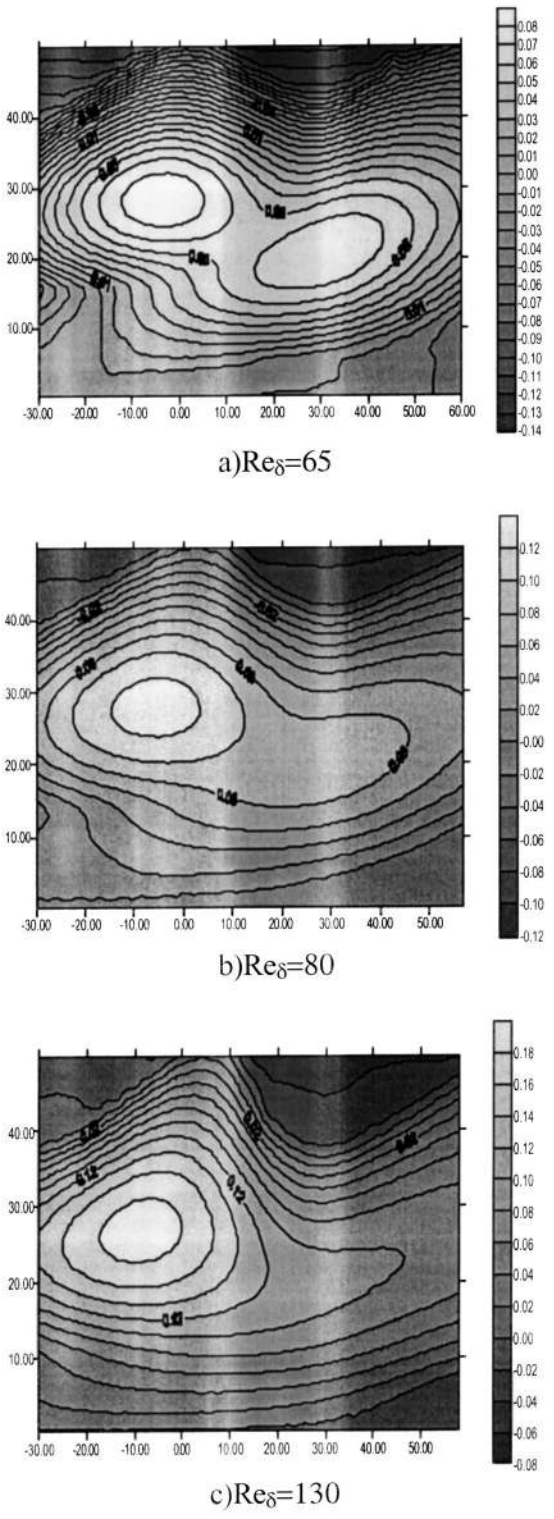

FIG. 3. Iso-lines of $\omega_i = \text{const}$ in the stationary disk boundary layer and at different local Reynolds numbers.

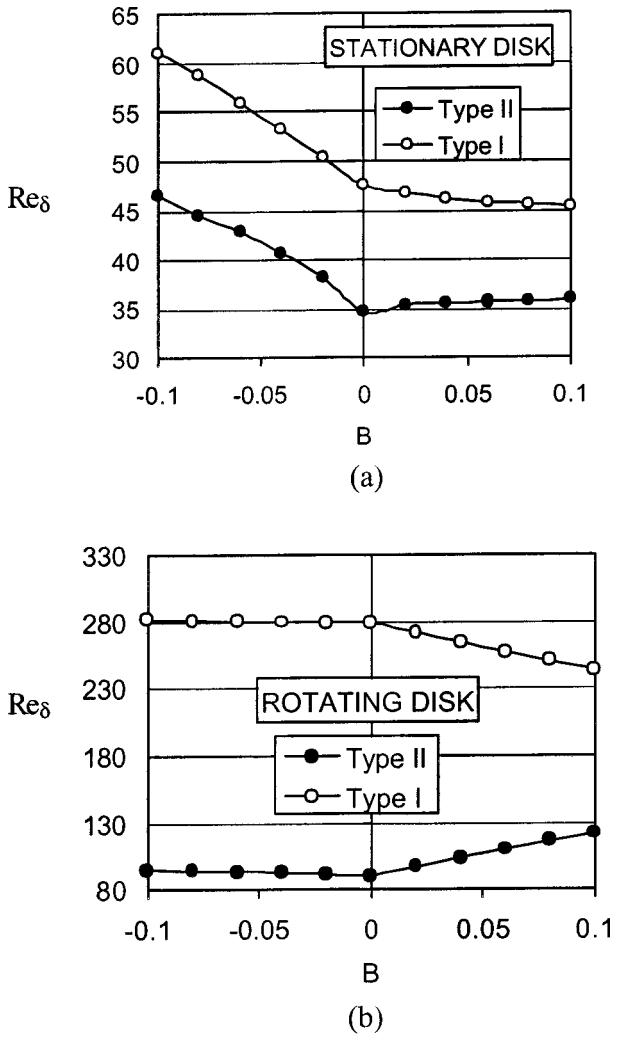

FIG. 4. Critical local Reynolds numbers versus the thermal Rossby number B obtained at $\mathrm{Re}=1000$ in the stationary disk boundary layer (a) and in the rotating disk boundary layer (b).

decreasing. The influence of cooling on the neutral curves is shown in Fig. 5. In contrast, when cooling the stator wall ($B<0$), all the type II characteristics parameters ($\lambda_r, \varepsilon, V_\phi$) decrease. A strong decrease of the inclination is noticed from $-35.3°$ ($B=0$) to $-23.7°$ ($B=-0.1$). As for $B>0$, the sign of the spiral arm's inclination for the type I changes for $B=-0.02$ but remains nevertheless in a smaller range of values than in the cooling of the rotor. The wavelength and the phase velocity remain almost constant when cooling the stator.

b. Rotating disk boundary layer. The type I and II critical Reynolds numbers versus B are shown in Fig. 4(b) for the rotating disk boundary layer.

We see that cooling of the rotating disk ($B>0$) stabilizes the flow with respect to type II instability. The critical Reynolds number, $\mathrm{Re}_{\delta\mathrm{II}}$, increases from 90.23 to about 128 when B is increased from 0 to 0.1. In contrast, the flow is destabilized at slightly lower Reynolds numbers with respect to type I instability for the same thermal boundary conditions ($B>0$): $\mathrm{Re}_{\delta\mathrm{I}}$ decreases from 278.6 to about 240 with increasing B from 0 to 0.1. This behavior is different from the usual results observed for the type I inflectional instability, where cooling stabilizes the boundary layers by lowering the inflectional point. However we can see from Fig. 2 that cooling of the rotating disk has negligible influence on the position of the inflectional point ($z=1$ corresponding to the rotating disk in Fig. 2). That is probably due to the complexity of this class of rotating non-isothermal flows. The influence

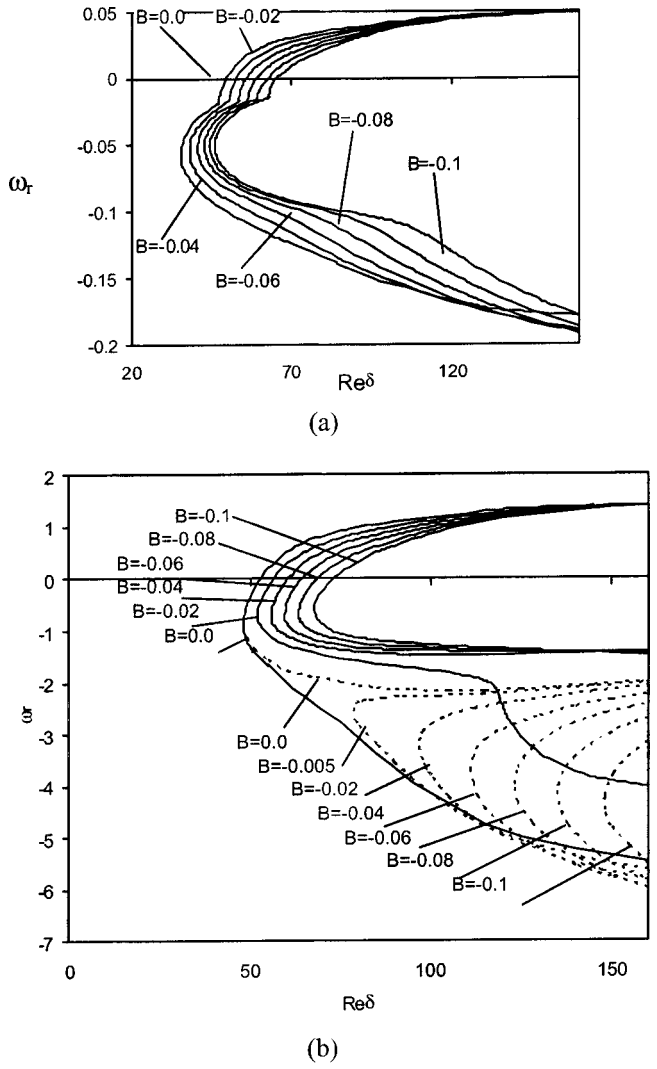

FIG. 5. Comparison of the neutral curves $\omega_r = f(\mathrm{Re}_\delta)$ in the stationary disk boundary layer obtained at different B: (a) convectively unstable areas, (b) absolutely unstable areas (dashed lines indicate second family).

of cooling is also visible in Fig. 6, where the neutral curves obtained for $B = 0.0$, 0.04, and 0.1 are presented.

The wavelength of the type II instability is slightly increased from 28.3 ($B = 0$) to 32.7 ($B = 0.1$), with a nearly constant inclination angle and phase velocity. In contrast for type I, the phase velocity is multiplied by a factor of 3 comparatively with the isothermal case but remains globally very slow, while the wavelength remains almost constant and the inclination angle of the spiral arms reduced by about 20%.

For $B < 0$, the thermal effect is small and does not involve any change in the critical Reynolds numbers [Fig. 4(b)]. This can be attributed to the small change in radial velocity (F) of the rotating disk boundary layer with B in the range between 0 and -0.1 (see Fig. 2). All the type II characteristics parameters ($\lambda_r, \varepsilon, V_\phi$) slightly decrease comparatively to the isothermal case while they remain almost constant for the type I.

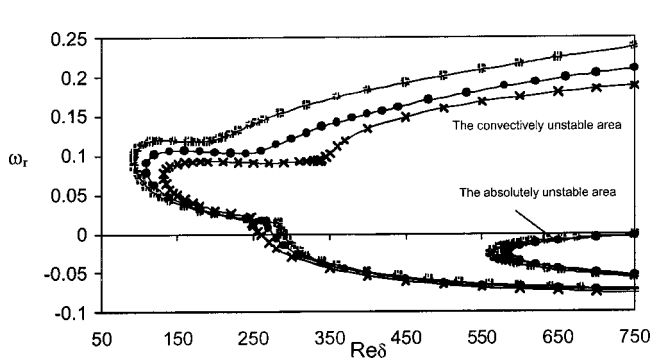

FIG. 6. Comparison of the neutral curves $\omega_r = f(\mathrm{Re}_\delta)$ of the absolutely and convectively unstable flow obtained for $B = 0.1$ (crosses), 0.04 (dots), and 0.0 (squares). The rotating disk boundary layer.

B. Convective/absolute instability

We use the Briggs[16] criterion with a fixed wave number in the azimuthal direction β to determine the region of absolute instability. All the critical parameters of the absolutely unstable area are presented in Tables VII and VIII for the stationary and rotating layer flows, respectively, together with literature results.

1. Stationary disk boundary layer

In the Bödewadt layer flow on a single disk, the agreement with Lingwood's results[18] is very good for all the critical parameters (Table VII). Lingwood obtained for the Bödewadt layer $\mathrm{Re}_{\delta \mathrm{a}} = 21.6$ whereas our critical Reynolds number of the absolutely unstable area obtained for the same geometry is $\mathrm{Re}_{\delta \mathrm{a}} = 21.7$. The comparison of the neutral curves of the convectively and absolutely unstable areas obtained for the Bödewadt flow (single disk model) is presented in Fig. 7(a). From Fig. 7(a) we can see that the almost the whole convectively unstable area in the Bödewadt flow is absolutely unstable. Next, the Lingwood model has been extended by considering the whole rotor-stator isothermal flow ($B = 0.0$). As in the case of the single disk, almost the entire convectively unstable flow on the stationary disk turned out to be absolutely unstable [see the neutral curve in Fig. 7(b)]. However, the critical Reynolds number of the absolutely unstable flow on the stationary disk has been found to be about two times larger than in a single disk case at $\mathrm{Re}_{\delta \mathrm{a}} = 48.5$.

2. Rotating disk boundary layer

In the Ekman boundary layer flow on a single disk, we obtained exactly the same results as those published by Lingwood, i.e., $\mathrm{Re}_{\delta \mathrm{a}} = 198$ (others critical parameters are presented in Table VIII). The comparison of the neutral curves of the convectively and absolutely unstable areas obtained for the Ekman flow (single disk model) is presented in Figs. 7(c). However, on the rotating disk (two-disks model), the critical Reynolds number of the absolutely unstable flow has been determined much larger at $\mathrm{Re}_{\delta \mathrm{a}} = 562$ which is more than 2.5 times larger than the value obtained in the Lingwood model of the Ekman flow, $\mathrm{Re}_{\delta \mathrm{a}} = 198$. That shows the strong influence of the stationary disk boundary layer flow on the critical Reynolds number of the rotating disk layer. As for type I and type II instabilities characteristics, we could expect that a more relevant comparison would be obtained by interpolating Lingwood's results at $\mathrm{Ro} = -0.751$ from her data obtained at $\mathrm{Ro} = -0.6$ and $\mathrm{Ro} = -0.8$. However, even if

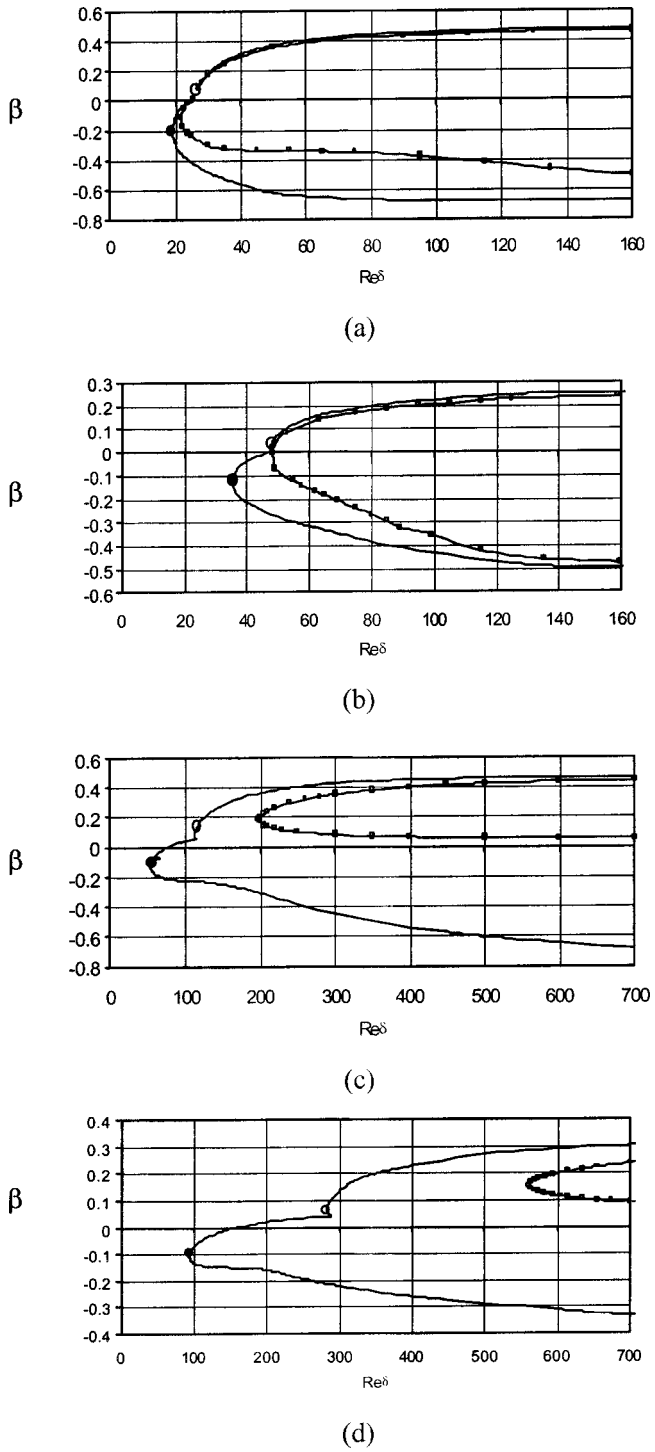

FIG. 7. Comparison of the neutral curves $\beta=f(\mathrm{Re}_\delta)$ of the absolutely (black squares) and convectively (solid line) unstable flow obtained for [(a) and (b)] the Bödewadt flow and the stationary disk boundary layer, respectively; [(c) and (d)] the Ekman flow and the rotating disk boundary layer, respectively. The critical points of type I and type II are marked by the white and black dots, respectively.

the comparison is better than in the Ekman layer case, the interpolation gives $\mathrm{Re}_{\delta \mathrm{ca}} \sim 400$, the difference between Lingwood's model and the two-disk model remains quite large. Because we have found a very good agreement with the results of Lingwood in the single disk case, we can only conclude that the effect of the stationary disk on the stability of the rotating disk boundary layer is not completely taken into account through this Rossby number. The neutral curves of absolutely and convectively unstable flow obtained for the rotating disk boundary layer are presented in Fig. 7(d). From the comparison in Figs. 7(c) and 7(d) we can see that for both models (the Ekman flow and the rotating disk boundary layer) the absolutely unstable flow exists only in a very narrow range of the spectral parameters not far from the upper branch of the type I neutral curve where inviscid type I instability is fully dominant. Type II appearing at lower Reynolds number than type I remains totally convectively unstable. (In Fig. 7 we marked the critical points of type I and type II by the white and black dots, respectively.)

3. Non-isothermal flow

In the next step, we extend our absolute/convective calculations to the non-isothermal class of flow. In Fig. 6 the neutral curves of convectively and absolutely unstable areas obtained for the rotating disk boundary layer and for the different thermal Rossby number are presented. From Fig. 6 we can see that cooling stabilizes the absolutely unstable areas of the rotating disk boundary layers, but this influence is not significant. Figure 5(b) shows the neutral curves of absolutely unstable flow obtained for the stationary disk boundary layer and for the different thermal Rossby numbers (solid line). Figure 5(b) presents also the second families of branch points with $\omega_i=0.0$ (dashed line). The nature of the second family of branch points was discussed in Lingwood.[18] As it was shown in Lingwood's paper, for larger value of Reynolds number, the branch points of the second family are not pinch point types. Only solid lines in Fig. 5(b) depict absolutely unstable areas. These areas decrease with cooling.

VI. NUMERICAL RESULTS (DNS)

Numerical investigations have been performed in a rotating cylindrical cavity of aspect ratio $L=5$. As we investigate the first stages of the transition to unsteadiness, the Reynolds numbers under consideration are not too large ($\mathrm{Re}_R < 14\,000$), and then spatial resolution $N\times M\times K=65\times 49\times 48$ in the r, z, and φ directions, respectively, constitutes a good compromise between required accuracy and computational cost as emphasized by Serre and Pulicani.[28] Moreover, the solution has shown to be mesh independent for all the Reynolds numbers considered. The time step incorporated is $\delta t=5\times 10^{-3}$.

The velocity fluctuations, used to display the structures related to boundary layer instabilities, are computed with respect to the average flow solution.

Numerical results will focus more on the stability of the stationary disk boundary layer which governs the transition in the rotor-stator flow (see LSA results above). Indeed, the rotating disk layer becomes absolutely unstable at a high local Reynolds number ($\mathrm{Re}_{\delta \mathrm{ca}}=562$), hardly reachable using DNS.

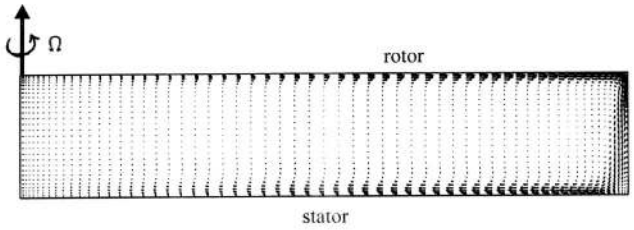

FIG. 8. Base flow. Velocity field in the meridional plane (r, z, 0) at $\mathrm{Re}_R=3000$. Batchelor-type flow composed of two boundary layers on the rotating and stationary disks separated by a solid body rotating core.

A. Base flow

At $\mathrm{Re}_R=3000$, the flow solution is steady, axisymmetric, and composed of boundary layers on each disk and of a central core flow in near solid body rotation. Batchelor[34] showed that the rotating disk drives the fluid below the disk into uniform rigid rotation by viscous effects. This uniformly rotating core then gives rise to a shear layer on the stationary disk: see in Fig. 8 the velocity field in the meridian plane (r, z, 0) at $\mathrm{Re}_R=3000$.

B. Transition to unsteadiness

The first bifurcation from the base flow to an unsteady state has been carefully analyzed using DNS results. That way, the rotation has been increased step by step from $\mathrm{Re}_R=3000$ by considering a small increment equal to 300. In contrast to most former studies in similar geometries, a supercritical Hopf bifurcation has been emphasized for a critical Reynolds number estimated in a range $11\,500 \leqslant \mathrm{Re}_R \leqslant 12\,300$.

We also repeat this procedure for the flow additionally disturbed by superimposing on the initial condition, at every consecutive Re_R, a three-dimensional perturbation function of general form $\eta \sin(p\varphi)$, where p is an arbitrary number corresponding to an azimuthal wavelength and η is the amplitude growth rate.[9,10] Calculations are performed for different values of η ($0.0 \leqslant \eta \leqslant 3.5$) and for only one value of $p=2\pi/4$. In a former study,[9] we found no influence of p on instability structures.

The behavior of the dependent variables is monitored in 15 points, in five different positions in the radial direction N ($\frac{1}{6}$, $\frac{1}{3}$, $\frac{1}{2}$, $\frac{2}{3}$, $\frac{5}{6}$) and in three positions in the axial direction M ($\frac{9}{10}$, $\frac{1}{2}$, $\frac{1}{10}$) corresponding to the stationary disk layer, the geostrophic core and the rotating disk layer, respectively. N and M are numbers of collocation points in the radial and axial directions, respectively. The monitoring points in the radial direction are marked by letters A, B, M, C, and D (Fig. 1).

1. Case without superimposed disturbance ($\eta=0$)

Let us consider first the case where the flow is only disturbed by the change of the disk rotation (change of Re_R). In this case, the flow becomes oscillatory at $\mathrm{Re}_R=12\,900$ and the oscillations over the stages of time considered remain slightly irregular.

The instability is much more intense in the stationary disk layer by an order of magnitude of 10^3 with respect to the corresponding rotating disk layer disturbances. As no disturbance can be transported from the stationary disk layer, due to the presence of a stable flow region around the axis where all the disturbances are damped ($\mathrm{Re}_\delta=35.5$), the rotating disk layer remains stable at this rotation and only very small oscillations can be emphasized.

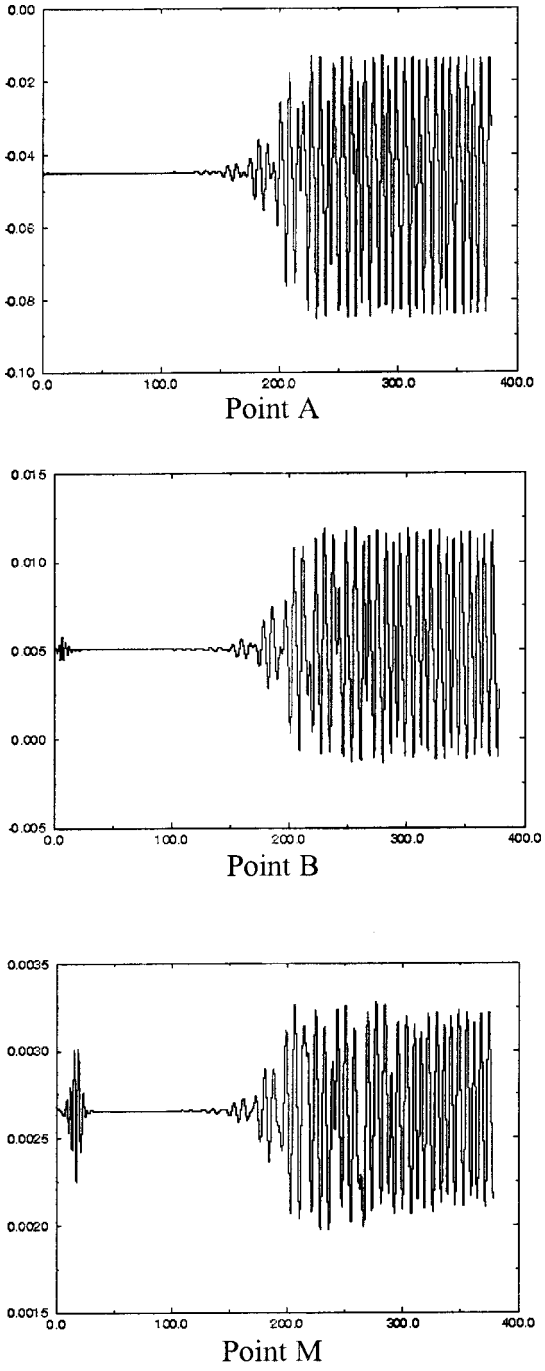

FIG. 9. Time histories of the axial component of the velocity in the stationary disk boundary layer at $\mathrm{Re}_R=13\,200$, $\eta=0$ and at different monitoring points A, B, M.

The oscillatory behavior is accurately investigated at slightly larger $\mathrm{Re}_R=13\,200$: Figs. 9 and 10 present time histories of the axial velocity component obtained at the monitoring points A, B, and M, in the stationary and rotating disk boundary layers, respectively. As expected by our LSA re-

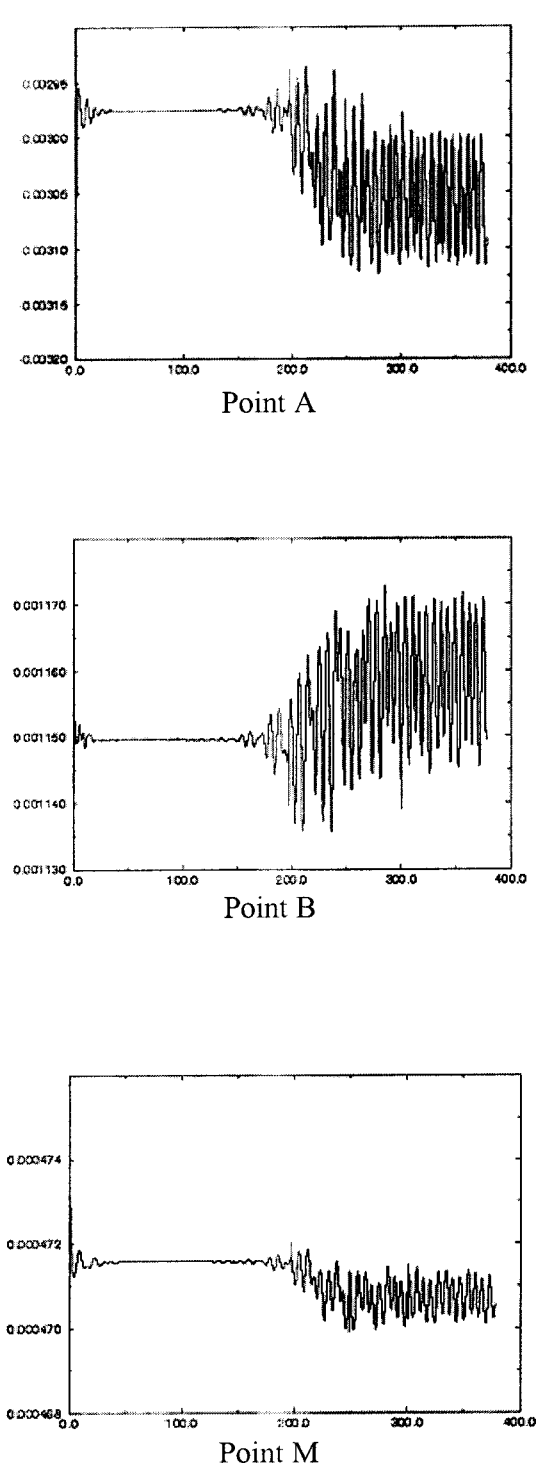

FIG. 10. Time histories of the axial component of the velocity in the rotating disk boundary layer at $\mathrm{Re}_R=13\,200$, $\eta=0$ and at different monitoring points *A*, *B*, *M*.

sults, the minimum of the oscillations amplitudes in both layers is reached in the near axis region, at the sampling points *C* and *D*, where the time histories show microscopic oscillations of amplitude less than 10^{-7}.

a. Stationary disk boundary layer. In the stationary disk boundary layer, the rotation change brings about a disturbance characterized by a wave packet which is rapidly damped ($t=20$), and then the flow looks reaching a steady state. Nevertheless, microscopic oscillations present during this steady state start exponentially growing at the same time ($t=150$) and at the all monitoring locations (Fig. 9). Finally, these oscillations reach an asymptotic finite-amplitude periodic state with a constant angular frequency $\sigma\sim 1.1$ ($\sigma=2\pi/\Delta t$), very close to the rotation frequency (Hopf bifurcation).

b. Rotating disk boundary layer. Exactly the same behavior is observed in the rotating disk boundary layer, i.e., the disturbance is first damped and finally an oscillatory solution appears. The angular frequency $\sigma\sim 0.82$ is slightly lower than in the stationary disk layer. Nevertheless, in contrast to the stator layer in which the perturbations oscillate around the steady state, the oscillations in the rotor layer are shifted in relation to the steady initial state solution. Consequently, this asymptotic periodic state breaks the centrosymmetry property in the rotating disk layer.

2. Case with superimposed disturbance ($\eta>0$)

Oscillatory solutions have been also observed for $\eta>0$, that is, when a 3D disturbance is superimposed to the flow. In this case, the flow becomes oscillatory at a slightly lower Reynolds number ($\mathrm{Re}_R=12\,300$) than with $\eta=0$ ($\mathrm{Re}_R=12\,900$). Moreover, the oscillations are very regular and the damping or the amplification processes of the instability are well established and purely periodic.

The time histories are presented in Fig. 11 at the monitoring point *A* in the stationary disk boundary layer, and for different Reynolds numbers $\mathrm{Re}_R=10\,200$, $11\,100$, $12\,300$ ($\eta=3.5$). At $\mathrm{Re}_R=10\,200$ and $\mathrm{Re}_R=11\,100$, oscillations of frequency $\sigma\sim 1.51$ are decaying exponentially, exhibiting stable solutions at these rotation rates during the considered computational time. At slightly larger Reynolds number, $\mathrm{Re}_R=12\,300$, the disturbances grow exponentially almost from the beginning of the time history. The frequency at the asymptotic finite amplitude oscillatory state is equal to 1.523, slightly larger than the one measured during the transient time at smaller Re_R. At all monitoring points in the stationary disk layer, the oscillatory solution is observed without any chaotic behavior and it is shown to be independent of the radial location (the differences between frequencies calculated at all monitoring points being less than 1%) except in the near axis region (points *C* and *D*) where the flow remains almost stable.

Disturbances of different growth rate η are shown to give exactly the same final amplitude state flows (Fig. 12). Comparison of the time histories obtained for various η at $\mathrm{Re}_R=13\,200$ and at the location *A* in the stationary disk layer shows that the frequency of the oscillatory final state is independent of the amplitude growth rate η ($\eta=0$, 2.0, and 3.5). However, the results show that the transient time to reach the stable state noticeably depends on η: $t=400$ for $\eta=0.5$, $t=150$ for $\eta=2$, $t=110$ for $\eta=3.5$. Then, this transitory time depends on the amplitude growth rate which behaves very roughly as η^{-1}. A similar behavior has been already observed for instabilities of rotating disk layers within a rotating cavity with radial throughflow[10] where the

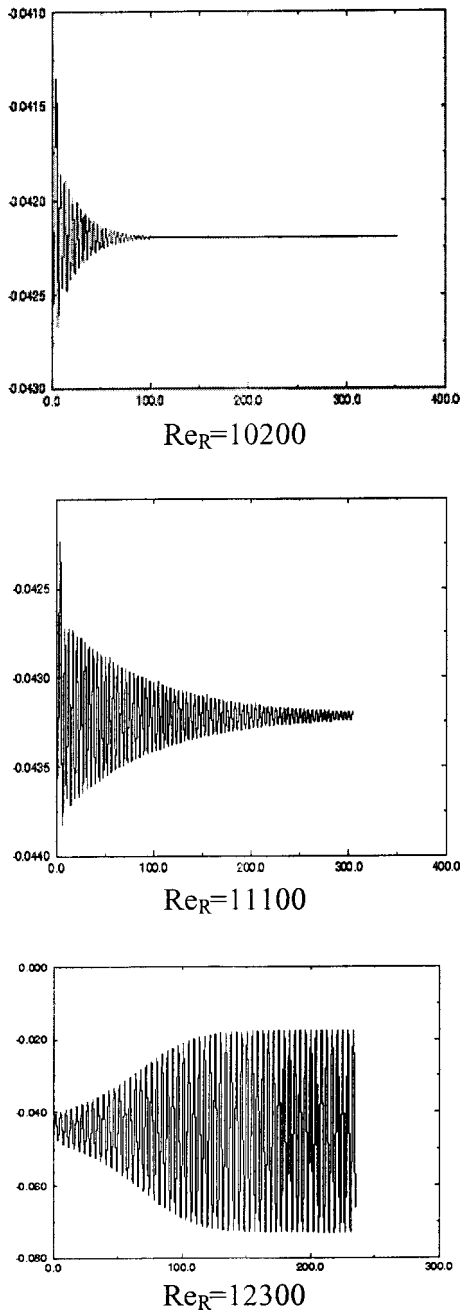

FIG. 11. Time histories of the axial component of the velocity in the stationary disk boundary layer at the monitoring point A and for different Reynolds numbers.

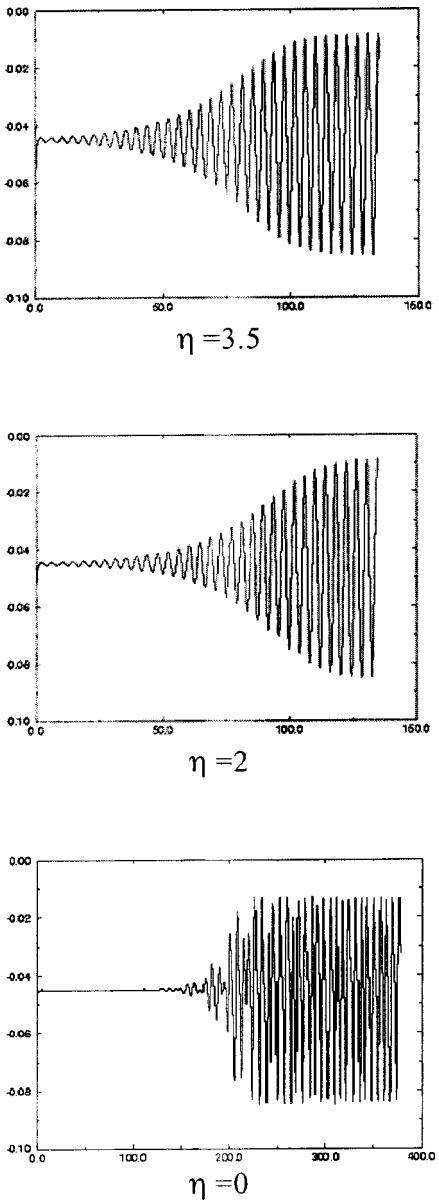

FIG. 12. Time histories of the axial component of the velocity at $\mathrm{Re}_R = 13\,200$ at the monitoring point A in the stationary disk boundary layer and for different values of η.

dependency of the transitory time with the growth rate was in this case as $\eta^{-1/3}$.

3. Critical Reynolds number

The exponential growth of the microscopic oscillations has been evaluated when increasing the rotation rate, starting from the base state previously described at $\mathrm{Re}_R = 3000$ and $\eta = 0$. The calculations show that duration of this exponential growth strongly depends on the Reynolds number and decrease when increasing the rotation rate; in the stator boundary layer, it needs $t = 230$ for $\mathrm{Re}_R = 12\,900$, $t = 140$ for $\mathrm{Re}_R = 13\,200$, t = 40 for $\mathrm{Re}_R = 13\,300$ and regular oscillations of constant frequency $\sigma \sim 1.08$ occur directly at the beginning of the time history for $\mathrm{Re}_R = 13\,500$. Due to large CPU time, it turned out impossible to reach a growing oscillatory solution for Reynolds numbers lower than 12 900 and consequently to determine precisely the critical Reynolds number for the unsteadiness. The difficulty in obtaining reliable data concerning the transition to unsteadiness, due to prohibitive integration time, was already reported in 2D calculations.[22] Nevertheless, by interpolating the different values of Reynolds numbers obtained in the present study (for $\eta = 0$), this critical Reynolds number can be estimated to be in a range between 11 500 and 12 300.

4. Stepping back effect

Calculations have been also performed in order to check the "stepping back" effect. Calculations have been carried out at $\mathrm{Re}_R = 12\,600$, 12 900, and 13 200 ($\eta = 0$) using as ini-

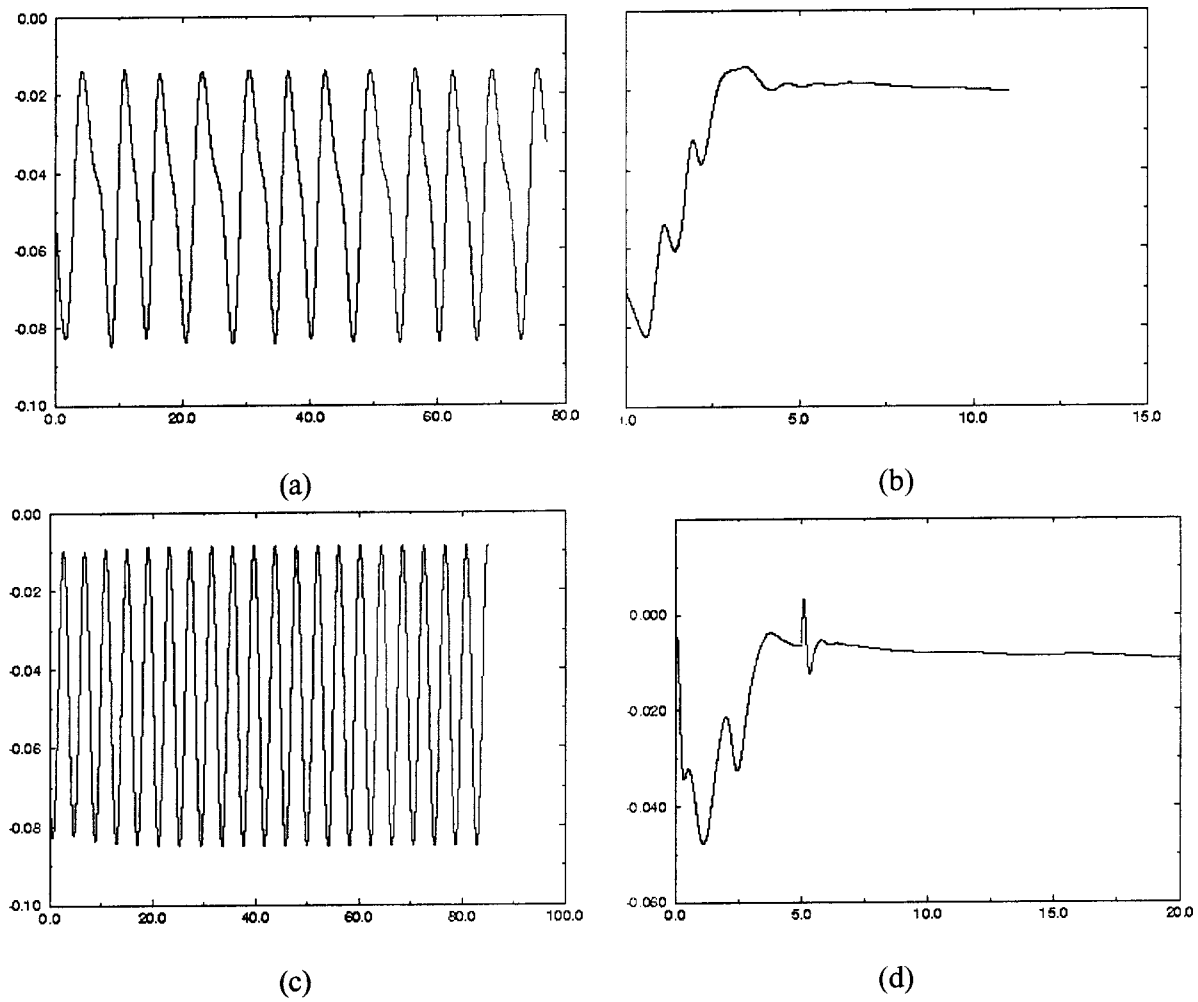

FIG. 13. (a) and (b) Time histories of the axial component of the velocity obtained at $\mathrm{Re}_R=13\,200$, $\eta=0.0$: (a) outer cylinder attached to the stator, (b) outer cylinder attached to the rotor and using (a) as initial condition. (c) and (d) Time histories obtained at $\mathrm{Re}_R=13\,200$, $\eta=3.5$: (c) outer cylinder attached to the stator; (d) linear azimuthal velocity profile as boundary condition and using (c) as initial condition.

tial conditions the instantaneous oscillatory state solutions obtained at $\mathrm{Re}_R=12\,900$, $13\,200$, and $13\,300$, respectively. No stepping back has been detected that supposes a supercritical bifurcation as reported in experiments.[6,8]

5. End-wall confinement and oscillatory solutions

Present computations show that the end-wall boundary layer strongly influences the transition to unsteadiness. Indeed, by changing the end-wall condition, the spatio-temporal characteristics of the stationary disk inflow are noticeably modified and, consequently, the stability of the boundary layer also.

The present results show that an end-wall attached to the rotor stabilizes the flow by switching from an oscillatory state (observed with an end-wall at rest) to a steady state at the same rotation rate. Indeed, calculations have been performed in two cases at the same rotation, $\mathrm{Re}_R=13\,200$, starting from the configuration with an end-wall at rest and using two other different end-wall boundary conditions:

(i) Without superimposed disturbance ($\eta=0$) and a rotating end-wall attached to the rotor. An exponential distribution of the azimuthal velocity ($v=(1-\exp(-z-1)/0.06)$) has then been considered. As an initial condition, we used the finite amplitude results presented above at $\mathrm{Re}_R=13\,200$ ($\eta=0.0$).

(ii) With a superimposed disturbance ($\eta=3.5$) and using a linear azimuthal velocity profile $v=(z+1)/2$ as the end-wall boundary condition. As initial condition, we used the finite amplitude results presented above at $\mathrm{Re}_R=13\,200$ ($\eta=3.5$).

Time histories at the monitoring point A obtained for cases (i) and (ii) are presented in Fig. 13 together with fragments of the time histories of initial conditions. These results clearly show the strong influence of the end-wall boundary condition on the stability of the stationary disk boundary layer. In both cases, the disturbances previously observed are quickly damped.

By changing an endwall at rest to a rotating one noticeably modifies the stationary disk layer on about a half from the end-wall. The flow becomes nonparallel and the boundary layer thickness increases when the radius decreases along about a half of the stationary disk, which obviously strongly influences the stability of the boundary layer. Two reasons

explain such modification in the structure of the stationary disk boundary layer. The first one is related to an increase of the vertical boundary layer thickness which develops along the end-wall when the end-wall rotates. Then, the impact region of the impinging axial jet on the stationary disk is larger in this configuration. The second reason is related to an increase of the azimuthal velocity in the core flow region located in the vicinity of the end-wall. Indeed, the azimuthal velocity noticeably increases with the radius, from the mid-cavity ($v^*/\Omega R_1 = 0.25$) to the end-wall ($v^*/\Omega R_1 = 1$). As the stationary disk boundary layer thickness is scaled on this core flow velocity, it decreases when the velocity increases.

The boundary layer flow in this part of the cavity is then profoundly modified and does not correspond to an actual Bödewadt layer (single disk flow) anymore. Consequently, its stability also changes and as it was the only part of the boundary layer which was unstable at the considered moderate rotation speed (because corresponding at the largest radii), the disturbances are damped.

C. Vortex structures related to stationary disk boundary layer instabilities

As in Ref. 9, the present DNS results show the existence of two types of instability structures: axisymmetric and three-dimensional structures which are related to type II and type I instabilities, respectively, by analogy to the linear stability results presented above. For all considered Reynolds numbers in this study, the rotating disk boundary has remained globally undisturbed (amplitudes of disturbances less than 10^{-6}) and consequently the stationary disk layer stability only is then discussed below. Solution without and with superimposed disturbance have been successively considered at two rotation rates, $\mathrm{Re}_R = 11\,100$ and $\mathrm{Re}_R = 13\,200$. Two-dimensional annular disturbances and 3D spiral vortices recognized as type II and type I instability have been observed.

Very close to the previously estimated critical Reynolds number of unsteadiness (Sec. VI), at $\mathrm{Re}_R = 11\,100$ ($\eta = 0$), the flow remains steady over the considered computational time and it would be much too expensive in terms of computational costs to reach an oscillatory state as we know that close to the threshold this time can be infinite. Nevertheless, a solution of very small amplitude already exists (about 10^{-4}) and microscopic oscillations can be emphasized in the time history. In spite of the low level of these disturbances, the solution yields two pairs of circular vortices near the stationary disk which show characteristic parameters in good agreement with those found for the type II instability by our LSA analysis (Table II). These two pairs of rolls are observed at local Reynolds numbers in a range $26.8 \leqslant \mathrm{Re}_\delta \leqslant 58.5$, and their radial wavelength is in a range $5.3 \leqslant \lambda_r \leqslant 10$ (with $\lambda_r = \Delta r / n_r$, where Δr is the radial length occupied by n_r rolls), corresponding to the critical parameters of type II.

In order to accelerate the occurrence of an oscillatory state, the solution has been disturbed at the same rotation rate $\mathrm{Re}_R = 11\,100$, using no zero values of η ($1.5 \leqslant \eta \leqslant 3.5$). As previously observed (Sec. VI), the solutions have been shown independent of the disturbance intensity η. Only spiral vortices are now observed in the stationary disk layer with characteristic parameters agreeing well with those found by LSA and related to type II instability (Table I). The train of vortices travels in the main flow direction with a radial phase velocity in the range $-0.0032 \leqslant V_{\phi r} \leqslant -0.002$ with $V_{\phi r} = \lambda_r \sigma / 2\pi\, \mathrm{Re}_\delta$, and expands in the azimuthal direction under the form of 12 spiral arms with an average negative angle equal to $\varepsilon = -15°$. These traveling structures only occur in the inflow at the radius $r^* = 3R_1/4$ and vanished at about $r^* = R_1/4$. Then, the stationary disk layer is only unstable in a flow region located between two radii corresponding to local Reynolds numbers $\mathrm{Re}_\delta = 23.4$–$74.6$. This result agrees well with linear stability analysis for type II (Sec. V) as this instability only exists in a narrow range of Re_δ.

Starting from the solution at $\mathrm{Re}_R = 11\,100$ ($\eta = 0$), the rotation has been suddenly increased to $\mathrm{Re}_R = 13\,200$. At this larger rotation rate, only spiral vortices related to type I instability are observed at the final oscillatory state in the stationary disk layer.

A relatively short time is required to reach the growing oscillatory solution (the time history is presented in Figs. 9 and 10). Except for the initial disturbance induced by the rotation speed increase which is quickly damped (at about $t = 30$), the flow looks stable until $t = 140$ where exponentially growing oscillations appear. At $t = 200$, the asymptotic finite amplitude state is finally obtained. However, enlargement of the time history between $30 \leqslant t \leqslant 100$ shows that microscopic oscillations already exist in this time range. In Figs. 14(a) and 14(b), vortex structures related to stationary disk layer instabilities are shown both during the transient ($t = 60$) and the final state ($t = 320$).

At $t = 60$, the solution is characterized by two pairs of circular vortices very similar to the ones observed at $\mathrm{Re}_R = 11\,100$ with radial wavelength $5.9 \leqslant \lambda_r \leqslant 14.7$, while at large radii 12 pairs of 3D spiral vortices expand in the azimuthal direction. These axisymmetric vortices, observed for radii corresponding to local Reynolds numbers in a range $25.8 \leqslant \mathrm{Re}_\delta \leqslant 62$, travel inward along the stationary disk layer with a radial phase speed $-0.02 \leqslant V_{\phi r} \leqslant -0.008$. As previously at $\mathrm{Re}_R = 11\,100$, these characteristic parameters agree well with our linear theory results related to type II instability of the stationary disk layer (Table I). At larger radius corresponding to a local Reynolds number $\mathrm{Re}_\delta = 64$, 3D spiral waves appear with an average angle of the spiral front equal to $\varepsilon = 13.2°$. Their radial wavelength and phase speed increase with the radius, in a range $7.3 \leqslant \lambda_r \leqslant 16.2$ and $-0.01 \leqslant \mathrm{V}_{\phi r} \leqslant -0.022$, respectively.

At $t = 320$, annular structures have disappeared and only spiral vortices definitively remain [Fig. 14(b)]. The critical Reynolds number of these spiral vortices has slightly decreased, compared to the transient state previously described, to a local radius corresponding to $\mathrm{Re}_\delta = 52.5$ and the average angle of the spiral front is now $\varepsilon = 12.1°$. The radial wavelength and the radial phase speeds of the stationary disk vortices are $4.4 \leqslant \lambda_r \leqslant 14.7$, $-0.0204 \leqslant \mathrm{V}_{\phi r} \leqslant -0.006$. All these characteristics parameters are in good agreement with the type I instability of the stationary disk layer found in our linear stability analysis (Table II).

A thin Taylor–Görtler-type vortex, related to the centrifugal instability of the vertical end-wall layer, can be also

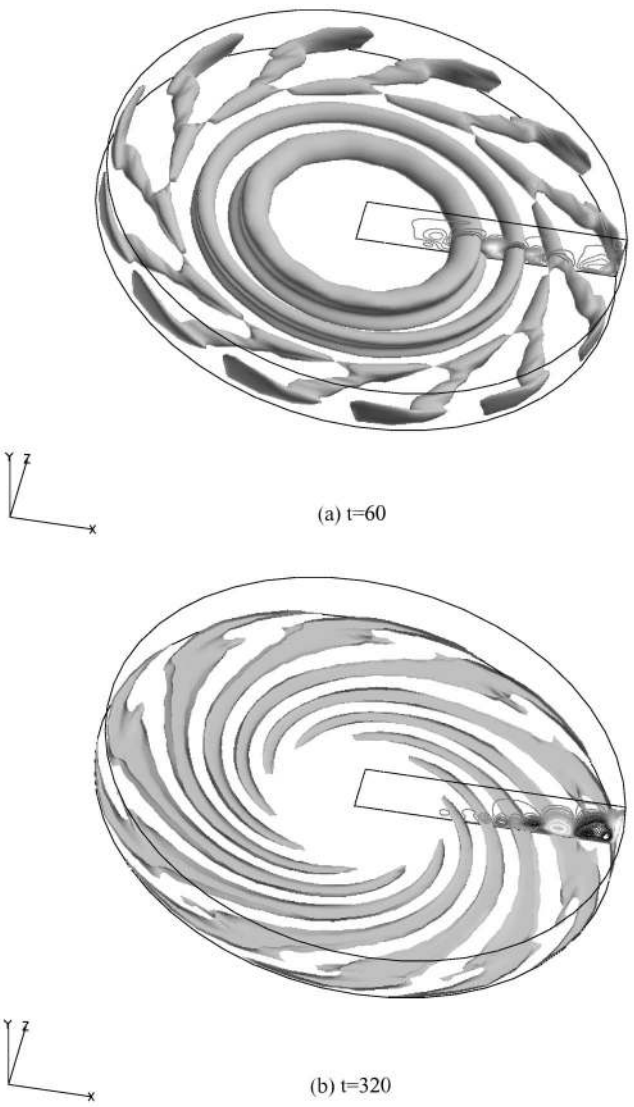

FIG. 14. Iso-surface of the fluctuations of the axial component of the velocity at $\mathrm{Re}_R=13\,200$, $\eta=0$. (a) Coexistence of annular and spiral structures related to stationary disk layer instability during the transient time $t=60$. (b) Final state showing only 12 spiral arms expanding in the azimuthal direction.

emphasized at the junction between the end-wall and the stator disk. This thin vortex is connected to spiral arms with a large angle $\varepsilon=26.5°$ which quickly decreases down to $\varepsilon=12.1°$ out the near end-wall region in order to join the spiral arms related to type I instability of the stationary disk layer. This structure is clearly visible in Fig. 15, where both spiral structures in the azimuthal direction and vortices in the meridian plane (r, z, ϖ) have been displayed in a Cartesian frame. In Fig. 16, an iso-surface of the axial component of the velocity displayed on the whole cavity height at $t=60$ shows that these spirals occur at the top of the end-wall layer, just where the flow turns from the centrifugal rotating disk layer, and expand to the geostrophic core flow region located close to the end-wall. This figure shows the quite large spatial extension of the flow region where this instability is located. These large spiral arms interact with the spiral arms related to the type I stationary disk layer instability

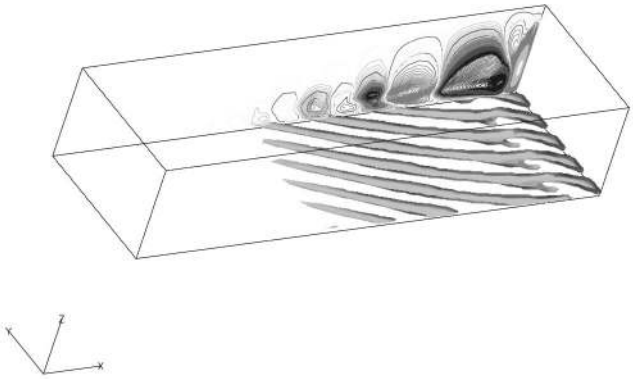

FIG. 15. Iso-surface of the fluctuations of the axial component of the velocity at $\mathrm{Re}_R=13\,200$, $\eta=0$, displayed in a Cartesian frame of reference showing the coexistence of two types of spiral related to the end-wall layer instability close to the vertical wall and to the stationary disk layer instability farther. Black arrows show the base flow direction.

previously described and not visible on this figure because it was located below.

Finally, the final state obtained at $\eta=0$ and described above has been disturbed at $\mathrm{Re}_R=13\,200$, using no zero values of η $(1.5\leqslant\eta\leqslant3.5)$. In contrast to the solution at lower rotation rate $\mathrm{Re}_R=11\,100$, the solution is stable relative to superimposed disturbances and there is no influence on the flow characteristics. About half of the stationary disk layer from the end-wall is unstable and vortices expand in the cavity under the form of 12 spiral vortices.

VII. DISCUSSION AND CONCLUDING REMARKS

This study is the first to provide linear stability analysis results (LSA) for a two-disk flow together with results from direct numerical simulations (DNS) obtained in a rotor-stator cavity of aspect ratio $L=5$ in order to accurately investigate the transition to unsteadiness. The study of the first stages of the transition process to turbulence is valuable because theoretical analysis is applicable and, coupled with high accurate DNS as here, allows an accurate description of the instability mechanisms which are known to play an important role in the breakdown process to turbulence.

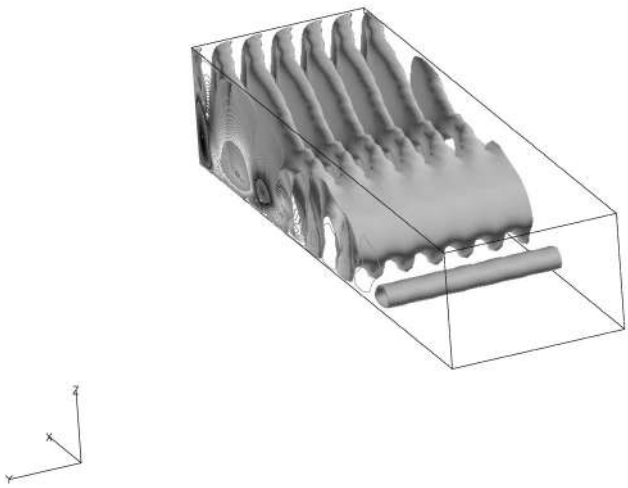

FIG. 16. Iso-surface of the fluctuations of the axial velocity component at $\mathrm{Re}_R=13\,200$, $\eta=0$, $t=60$, showing large spiral arms expanding from the vertical boundary layer to the geostrophic core and related to a centrifugal instability.

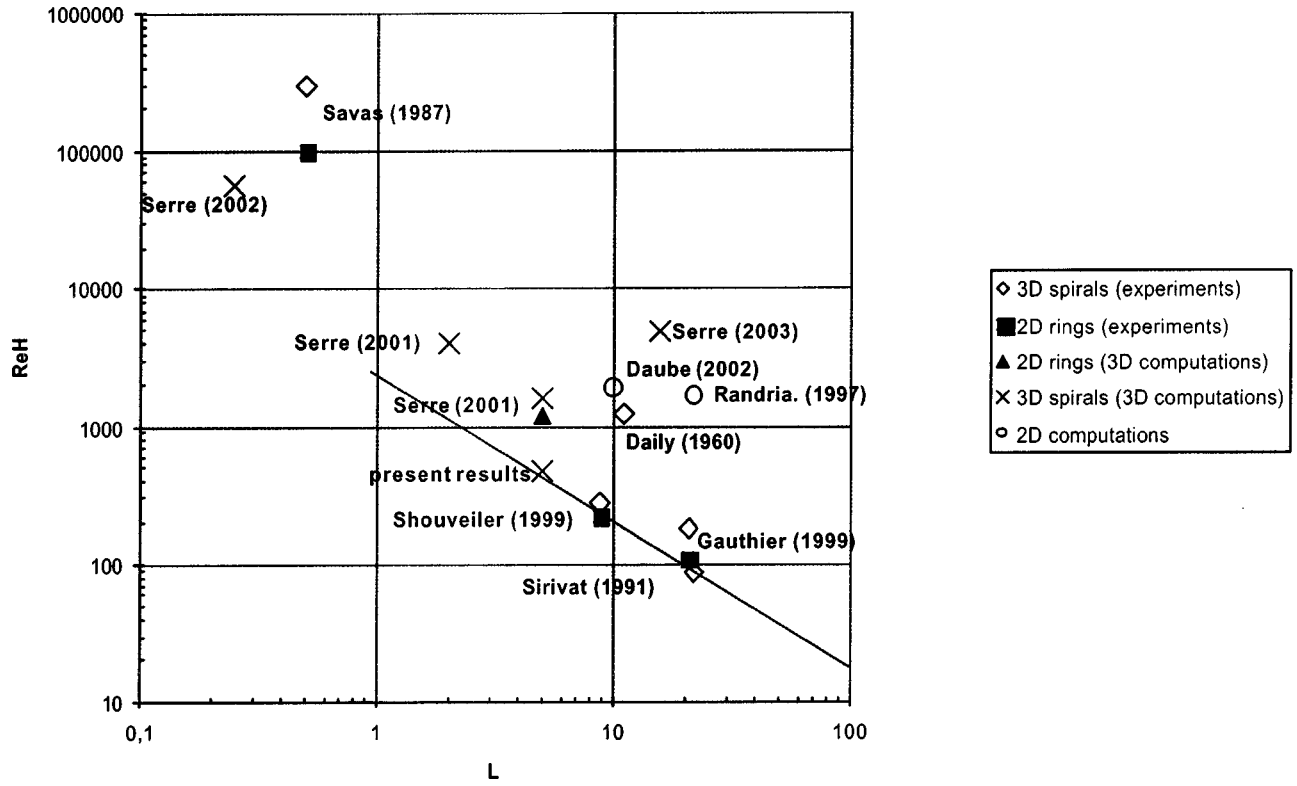

FIG. 17. Diagram of various numerical and experimental results in the plane (Re_H,L). The dashed line gives a lower limit to transition to unsteadiness.

(i) Surprisingly, no transition from a steady Batchelor state to an unstable oscillatory flow has been numerically emphasized until now,[9,35,36] except in cavities of small aspect ratio $L=2$.[9,22] In contrast, although it is technically difficult to emphasize such transition experimentally, the flow being very sensitive to external noises, recent experiments[8,9] have reported spiral structures and Hopf bifurcation from a steady state to a periodic flow. Then, we have decided to focus on the first bifurcation of the flow to a time-dependent regime and accurately characterize instability structures observed close to the threshold. Starting from a base state at $\mathrm{Re}_R=3000$ and increasing very slowly the disk rotation (steps of 300), this study has emphasized a Hopf bifurcation to an oscillatory solution of frequency $\sigma\sim 1.55$, and at a critical Reynolds number estimated between 11 500 and 12 300. This value of the frequency is in good agreement as well with the values obtained by LSA for the type II instability of the stationary disk layer as with the values measured experimentally[8] in a flow region not too far from the axis ($1\leqslant\sigma\leqslant 2$), corresponding to a radial extension close to the one considered in the present study with $L=5$. Note, also, that in the case of a fluid rotating at Ω over a single stationary and infinite disk, Lingwood[18] found theoretically $\sigma=1.3$ at the convective/absolute transition in the Bödewadt layer. Moreover, the absence of a stepping back effect seems to show that this bifurcation would be of supercritical type. As expected, the unsteadiness first develops in the stator boundary layer while the rotor boundary has remained stable for the rotation rates considered in this work.

(ii) In order to understand why no oscillatory state has been obtained in former numerical studies for such value of the aspect ratio, we have reported on the same graphics in Fig. 17 different numerical and experimental studies of the literature in terms of aspect ratio L and Reynolds number $\mathrm{Re}_\mathrm{H}=\Omega(2h)^2/\nu$. This Reynolds number is relevant for such comparison because it characterizes the base state just before the transition by scaling the thickness scale of the rotating disk layer on the cavity height. Then large values are typical of separated layers while small values are characteristic of the merged boundary layers regime. Numerical computations performed till now were mainly axisymmetric[35,36] and the results reported in Fig. 17 show that the critical value of unsteadiness is noticeably much larger than the one observed in the present study or in experiments. We even notice that the critical values obtained in the cases of 2D computations[35,36] are close to the ones given for transitional turbulent flow in experiments by Daily and Nece[37] or in recent 3D computations by Serre *et al.*[24] Axisymmetric assumption and the use of a rotating end-wall in these studies (stabilizing the flow coming from the rotating disk layer) can only explain such differences in the occurrence of unsteadiness. A line has been drawn for an aspect ratio L in a range 1 to 100 in order to show the good agreement obtained on

the critical value of Re_H between experiments and the present study, relative to the aspect ratio. For $L<1$, some values are reported for information only because the base flow is not of Batchelor type anymore, its stability being mainly governed by centrifugally unstable end-wall vertical layer. Concerning our former 3D computations[9] in the same geometrical configuration, the critical Reynolds number is also far enough above the threshold line. Indeed, in this work we focused on the characteristics of the structures related to boundary layer instabilities in highly unstable flows and not on an accurate evaluation of the threshold as in the present study.

(iii) The present computations have shown that a quite large part of the stationary disk boundary layer is influenced by the end-wall flow. Using rotating end-wall condition, the vertical end-wall layer impinges on the stationary disk and introduces nonparallel effects. As the end-wall effects go to mid-radius, where the local Re criterion was verified, it is then required to increase the rotation in order to get the transition and to attain a critical Re corresponding to a lower radius value—that is in the un-affected area. Nevertheless, in that case where the transition is obtained at smaller radius than mid-radius, the entire stator flow is destabilized, that is even in the end-wall driven region. The interaction between these phenomena is interpreted as being at the origin of the chaotic behavior in the entire stator layer.

(iv) Three-dimensional structures related to the stationary disk boundary layer instabilities have been accurately emphasized by DNS and studied using LSA results. Spiral arms with positive and negative angles have been observed in the stationary disk layer flow in good agreement with the LSA results. Annular structure already observed in experiments[6,8,15] and in computations[9] have been shown unstable in this configuration and only observed during the transient time before reaching the asymptotic oscillatory state. Taylor–Görtler-type vortices have also been observed at the junction between the stationary shroud and the stator expanding in near end-wall flow region under the form of large spiral arms.

DNS and LSA results agree very well and are summarized with selected results already published in the literature in Tables I–VIII.[38] Comparison between these results has shown that all the structures observed in the stationary disk layer by DNS are related to the generic type I and type II instabilities theoretically found by LSA.

(v) The absolute and convective nature of both rotating and stationary disk layers has been investigated by LSA (Sec. V). A study based on DNS of the global behavior corresponding to the absolute instability of the rotor-stator flow requires intensive and careful analysis (see the recent work of Davis and Carpenter[39] in the linear case of the Ekman layer) and is beyond the scope of the present work. Nevertheless, the present DNS results at $Re=13\,200$, $\eta=0$ provide in comparison with our LSA absolute/convective results (Sec. V) some additional interesting insights concerning the spatio-temporal behavior of instability disturbance. Indeed, the calculations have shown that the amplitude of the disturbances grows with the radius in both rotating and stationary disk boundary layers (as shown in Figs. 9 and 10) while the two base flow directions develop oppositely (see also Fig. 15). The amplitude of fluctuations reaches maximum in the near end-wall flow region corresponding to the monitoring point A (about 6×10^{-2} in the stator and about 10^{-5} in the rotor) while its minimum is reached at mid-radius at the monitoring point M (about 10^{-3} on the stator and about 10^{-6} on the rotor). Amplitude considered as equal to zero is monitored in the near axis region (point D). According to the amplitude level measured in the rotor layer (10^3 smaller than in the stator layer), the disturbances are only related to a noise which is amplified when it is convected by the base flow towards the end-wall. In the stationary disk layer, the structures disappeared at a radius corresponding to local Reynolds number equal to $Re_{\delta a}=52.5$ (Fig. 15), which is very close to the critical Reynolds number of the absolutely unstable area, $Re_{\delta a}=48.5$, obtained using LSA.

Moreover, in the rotating boundary layer, our linear two-disk results have shown that the critical Reynolds number of the absolutely unstable is $Re_{\delta a}=562$. The large difference observed between present LSA and Lingwood's results, especially in the case of the rotating disk boundary layer, justifies the two disks model here developed. Computations carried out by Serre *et al.*[24] in transitional turbulent regimes in an annular rotor-stator flow have shown coherent spiral vortices at a local Reynolds number Re_δ equal to about 500: this result brings some assessments to the critical value $Re_{\delta a}=562$ obtained in the present LSA. More additional investigations are then required using DNS, in order to explore the absolutely unstable area of the rotating disk boundary layer and to detail especially the connections between absolute instability and breakdown process to turbulence. Besides, intensive computations are already in progress in an open rotating cavity with radial through flow as the one described in Ref. 10.

(vi) LSA calculations have been already extended to non-isothermal flow ($-0.1\leqslant B\leqslant0.1$) in Sec. V. The results show that thermal conditions do alter the critical Reynolds numbers of the convectively and absolutely unstable area and in different ways the type I and type II instability characteristics. The instabilities look more affected in the stationary disk layer flow by thermal buoyancy than in the rotating disk layer flow where the rotating driven buoyancy is certainly larger and dominates the thermal effects for this range of B considered in the study. An important feature in the stationary disk layer flow is the change in the spiral

inclination from a negative angle in the isothermal case to a positive one as soon the rotor starts to be cooled. Further investigations are in progress for larger $\Delta T/T$ range where former natural convection results have empirically shown the extension of the Boussinesq approximation to be further valid.

ACKNOWLEDGMENTS

The authors are grateful to Professor P. Huerre and Professor J. M. Chomaz (LadHyX, Ecole Polytechnique) for fruitful discussions. The authors acknowledge financial support from CNRS for the stay in Marseille of E.T.-S. The computations were carried out on the Nec SX5 supercomputer from IDRIS CNRS Computing Center and partly in the Poznan University Computer Center.

[1] J. M. Owen and R. H. Rogers, "Heat transfer in rotating disc systems," in *Rotating Cavity*, edited by W. D. Morris (Wiley, New York, 1995), Vol. 2.
[2] R. Kobayashi, Y. Kohama, and C. H. Takamadate, "Spiral vortices in boundary layer transition region on a rotating disk," Acta Mech. **35**, 71 (1980).
[3] R. Lingwood, "Absolute instability of the boundary layer on a rotating disk," J. Fluid Mech. **299**, 17 (1995).
[4] R. Lingwood, "Experimental study of absolute instability of the rotating-disk boundary layer flow," J. Fluid Mech. **314**, 373 (1996).
[5] B. Pier, "Finite amplitude crossflow vortices, secondary instability and transition in the rotating disk boundary layer," J. Fluid Mech. **487**, 315 (2003).
[6] G. Gauthier, P. Gondret, and M. Rabaud, "Axisymmetric propagating vortices in the flow between a stationary and a rotating disk enclosed by a cylinder," J. Fluid Mech. **386**, 105 (1999).
[7] M. Itoh, "On the instability of the flow between coaxial rotating disks," in *Boundary Layer Stability and Transition to Turbulence*, ASME FED **114**, 83 (1991).
[8] L. Schouveiler, P. Le Gal, M. P. Chauve, and Y. Takeda, "Spiral and circular waves in the flow between a rotating and a stationary disc," Exp. Fluids **26**, 179 (1999).
[9] E. Serre, E. Crespo del Arco, and P. Bontoux, "Annular and spiral patterns in flow between rotating and stationary disks," J. Fluid Mech. **434**, 65 (2001).
[10] E. Serre, S. Hugues, E. Crespo del Arco, A. Randriamampianina, and P. Bontoux, "Axisymmetric and three-dimensional instabilities in an Ekman boundary layer flow," Int. J. Heat Fluid Flow **22**, 82 (2001).
[11] A. J. Faller, "Instability and transition of the disturbed flow over a rotating," J. Fluid Mech. **230**, 245 (1991).
[12] D. Lilly, "On the instability of Ekman boundary flow," J. Atmos. Sci. **23**, 481 (1966).
[13] A. J. Faller, "An experimental study of the instability of the laminar Ekman boundary layer," J. Fluid Mech. **15**, 560 (1963).
[14] D. R. Caldwell and C. Van Atta, "Characteristics of Ekman boundary layer instabilities," J. Fluid Mech. **44**, 79 (1970).
[15] O. Savas, "Stability of Bödewadt flow," J. Fluid Mech. **183**, 77 (1987).
[16] R. W. Briggs, *Electron-Stream Interaction with Plasmas* (MIT Press, Cambridge, 1964).
[17] P. Huerre and P. A. Monkewitz, "Local and global instability in spatially developing flows," Annu. Rev. Fluid Mech. **22**, 473 (1990).
[18] R. J. Lingwood, "Absolute instability of the Ekman layer and related rotating flows," J. Fluid Mech. **331**, 405 (1997).
[19] E. Tuliszka-Sznitko, E. Serre, and P. Bontoux, "On the nature of the boundary layers instabilities in a flow between a rotating and a stationary disc," C. R. Mec. **30**, 90 (2002).
[20] D. Dijkstra and G. van Heijst, "The flow between finite rotating discs enclosed by a cylinder," J. Fluid Mech. **128**, 123 (1983).
[21] M. L. Adams and A. Szeri, "Incompressible flow between finite discs," J. Appl. Mech. **49**, 1 (1982).
[22] N. Cousin-Rittemard, O. Daube, and P. Le Quéré, "Sur la nature de la première bifurcation des écoulements interdisques," C. R. Acad. Sci., Ser. IIb: Mec., Phys., Chim., Astron. **326**, 359 (1998).
[23] J. M. Lopez and P. Weidman, "Stability of stationary endwall boundary layers during spin-down," J. Fluid Mech. **326**, 373 (1996).
[24] E. Serre, P. Bontoux, and B. Launder, "Direct numerical simulation of transitional turbulent flow in an enclosed rotor-stator cavity," Int. J. Flow, Turb. Combust. **69**, 35 (2002).
[25] E. Serre and P. Bontoux, "Vortex breakdown in a three-dimensional swirling flow," J. Fluid Mech. **459**, 347 (2002).
[26] A. H. Hadid, "Chaotic flow in rotating lid cavities," Phys. Fluids A **5**, 1939 (1993).
[27] R. Peyret, *Spectral Methods for Incompressible Viscous Flow*, Applied Mathematical Sciences Vol. 148 (Springer, New York, 2002).
[28] E. Serre and J. P. Pulicani, "A three-dimensional pseudospectral method for rotating flows in a cylinder," Comput. Fluids **30**, 491 (2001).
[29] I. Raspo, S. Hugues, E. Serre, A. Randriamampianina, and P. Bontoux, "Spectral projection methods for the simulation of complex three-dimensional rotating flows," Comput. Fluids **31**, 745 (2002).
[30] E. Tuliszka-Sznitko and C. Y. Soong, "Instability of non-isothermal flow between coaxial rotating disks," in Proceedings of European Congress on Computational Methods in Applied Sciences and Engineering, Barcelona (2000).
[31] P. Huerre, "Open shear flow instability," in *Perspectives in Fluid Dynamics*, edited by G. K. Batchelor, H. K. Moffatt, and M. G. Worster (Cambridge University Press, Cambridge, 2000).
[32] K. Kupfer, A. Bers, and A. Ram, "The cusp map in the complex-frequency plane for absolute instabilities," Phys. Fluids **30**, 3075 (1987).
[33] F. Feria, "Axisymmetric instabilities of Bödewadt flow," Phys. Fluids **12**, 1730 (2000).
[34] G. K. Batchelor, "Note on the class of solutions of Navier–Stokes equations representing steady rotationally-symmetric flow," Q. J. Mech. Appl. Math. **4**, 29 (1951).
[35] O. Daube and P. Le Quéré, "Numerical investigation of the first bifurcation for the flow in a rotor-stator cavity of radial aspect ratio 10," Comput. Fluids **31**, 481 (2002).
[36] A. Randriamampianina, L. Elena, J. P. Fontaine, and R. Schiestel, "Numerical prediction of laminar, transitional and turbulent flows in shrouded rotor-stator systems," Phys. Fluids **9**, 1696 (1997).
[37] J. W. Daily and R. E. Nece, "Chamber dimension effects on induced flow and frictional resistance of enclosed rotating disks," Trans. ASME, J. Basic Eng. **82**, 217 (1960).
[38] M. V. Melander, "An algorithmic approach to the linear stability of the Ekman layer," J. Fluid Mech. **132**, 283 (1983).
[39] C. Davies and P. W. Carpenter, "Global behavior corresponding to the absolute instability of the rotating-disc boundary layer," J. Fluid Mech. **486**, 287 (2003).